

Intermediate mass Higgs bosons of the Minimal Supersymmetric Standard Model at the proposed CERN LEP \otimes LHC ep collider¹

Ghadir Abu Leil^a and Stefano Moretti^{a,b,2}

*a) Department of Physics, University of Durham,
South Road, Durham DH1 3LE, U.K.*

*b) Dipartimento di Fisica Teorica, Università di Torino,
and INFN, Sezione di Torino,
V. Pietro Giuria 1, 10125 Torino, Italy.*

Abstract

The production of the \mathcal{MSSM} Higgs bosons H^0, h^0, A^0 and H^\pm , in the intermediate mass range of the A^0 , at two different values of $\tan\beta$, is studied at the possible CERN LEP \otimes LHC ep collider, through γp interactions, by photons generated via Compton back-scattering of laser light. Signatures in which $H^0, h^0, A^0 \rightarrow b\bar{b}$ and $H^\pm \rightarrow \tau\nu_\tau$ are considered. Flavour identification on b -jets is assumed. Backgrounds to Higgs signals are computed. Explicit formulae for the helicity amplitudes of the Higgs processes are given.

¹Work supported in part by Ministero dell' Università e della Ricerca Scientifica (S.M.), by University of Durham Studentship and by World Lab. Fellowship ICSC (G.A.L).

²Address after September 1995: Cavendish Laboratory, University of Cambridge, Madingley Road, Cambridge, CB3 0HE, U.K.

Introduction

We know that, despite its innumerable experimental successes, the Standard Model (\mathcal{SM}) [1] cannot be a fundamental theory valid up to an arbitrary³ energy scale Λ . It should rather be regarded as an effective low energy model, which has to be replaced at an energy close to the Fermi scale $G_F^{-1/2} \approx 300$ GeV by some more fundamental theory. This can be seen from the fact that, for $\Lambda \gg G_F^{-1/2}$, the one-loop radiative corrections to the \mathcal{SM} Higgs mass M_ϕ are quadratically divergent (naturalness or hierarchy problem) [2].

Supersymmetric (\mathcal{SUSY}) models can solve this. The most intriguing among them is probably the Minimal Supersymmetric Standard Model (\mathcal{MSSM}) [3]. It incorporates two complex Higgs doublets of fundamental scalar fields (H_1^0, H_1^-) and (H_2^+, H_2^0), which, after a spontaneous symmetry breaking, originate five Higgs bosons: the \mathcal{CP} -even neutral H^0 and h^0 , the \mathcal{CP} -odd neutral A^0 and the charged H^\pm 's⁴. The attractions of the \mathcal{MSSM} are numerous. It is a predictive model: all masses and couplings in the Higgs sector can be expressed at tree-level in terms of only two real parameters, the ratio of the vacuum expectation values v_1 and v_2 of the two doublets (i.e., $\tan \beta = \frac{v_2}{v_1}$) and the mass of one of the bosons (e.g., M_{A^0}), and, at the same time, the radiative corrections can be kept well under control. It breaks the gauge symmetry close to the electroweak scale $G_F^{-1/2}$ and, if combined with Grand Unification Theories (\mathcal{GUT}), it predicts a value for the Weinberg angle θ_W in good agreement with the measured one and a value for the Grand Unification Mass $M_{\mathcal{GUT}}$ which can explain the not-observed proton decay [4]. It supplies a natural candidate for the dark matter in terms of the Lightest Supersymmetric Particle (\mathcal{LSP}), which is stable, neutral and weakly interacting (i.e., neutralino). Finally, so far, it survived stringent experimental constrains: e.g., the most part of its parameter space has not yet been excluded by LEP data [5].

While upper limits on the \mathcal{MSSM} Higgs boson masses can be deduced by arguments connected with the request of unitarity of the theory, which implies that at least one neutral \mathcal{MSSM} Higgs must have mass below ~ 1 TeV [6, 7, 8], lower limits can be extracted at present colliders. From LEP I ($\sqrt{s_{ee}} = M_{Z^0}$) experiments, as a result of searches for $e^+e^- \rightarrow Z^{0*}h^0$ and $e^+e^- \rightarrow h^0A^0$ events, one obtains [5]

$$M_{h^0} \gtrsim 44.5 \text{ GeV} \quad \text{and} \quad M_{A^0} \gtrsim 45 \text{ GeV}. \quad (1)$$

Extensive studies have been carried out on the detectability of \mathcal{MSSM} Higgs particles by the next generation of high energy machines, both at a pp hadron collider [6, 9, 10] and at an e^+e^- Next Linear Collider (NLC) [6, 11, 12, 13, 14, 15].

The region $M_{A^0} < 80 - 90$ GeV will be studied at LEP II ($\sqrt{s_{ee}} = 170 - 190$ GeV), by the Higgs decay channel $b\bar{b}$ [11], via one or both the processes $e^+e^- \rightarrow Z^{0*} \rightarrow Z^0h^0$ (bremsstrahlung) and $e^+e^- \rightarrow Z^{0*} \rightarrow h^0A^0$ (neutral pair production) [16].

Higgses with larger masses will be searched for at pp colliders like the LHC⁵, with $\sqrt{s_{pp}} =$

³A scale which has to be less than the Plank scale $M_{Plank} \sim 10^{19}$, where a description which includes quantum gravity is needed.

⁴The three neutral Higgs states of the \mathcal{MSSM} will be collectively indicated by the symbol Φ^0 .

⁵Since the most part of the results on Higgs searches at the SSC can be transposed to the LHC, in the following we will arbitrarily confuse the two bibliographies on this argument, even though we know that the SSC project has been definitely set aside.

10, 14 TeV and $\mathcal{L} \approx 10 - 100 \text{ fb}^{-1}$, or at e^+e^- NLCs, with $\sqrt{s_{ee}} = 300 - 2000 \text{ GeV}$ and $\mathcal{L} \approx 10 - 20 \text{ fb}^{-1}$.

At the LHC, because of the huge QCD background, the mass range $80 \text{ GeV} \lesssim M_{\Phi^0} \lesssim 130 \text{ GeV}$ is the most difficult to study since in this case a neutral Higgs boson mainly decays to $b\bar{b}$ pairs, for a large choice of the \mathcal{MSSM} parameters. However, studies have shown that the discovery of a neutral Higgs boson via the $\Phi^0 \rightarrow \gamma\gamma$ mode at hadron colliders can be exploited for the discovery of H^0 for $80 \text{ GeV} \lesssim M_{A^0} \lesssim 100 \text{ GeV}$ and of h^0 for $M_{A^0} \gtrsim 170 \text{ GeV}$, at all $\tan\beta$. For heavier masses, the ‘‘gold-plated’’ decay channel ($\Phi^0 \rightarrow 4\ell$) is useful for the H^0 if $\tan\beta \lesssim 7$ and $100 \text{ GeV} \lesssim M_{A^0} \lesssim 300 \text{ GeV}$, but not for the h^0 because of its too light mass⁶. Recently, it has been also shown [17] that with the b -tagging capabilities [18] of the LHC experiments⁷, it might be possible to rely, over a substantial portion of the parameter space, on the $t\bar{t}\Phi^0$ production channel, with one t decaying semileptonically and $\Phi^0 \rightarrow b\bar{b}$, for $80 \text{ GeV} \lesssim M_{\Phi^0} \lesssim 130 \text{ GeV}$, for at least one of the \mathcal{MSSM} Higgses h^0 or H^0 , removing the ‘‘window of unobservability’’ for $100 \text{ GeV} \lesssim M_{A^0} \lesssim 170 \text{ GeV}$ and $\tan\beta \gtrsim 2$, which remained in previous analyses. Moreover, it has been found [19] also that the reaction $bg \rightarrow bZ^0\Phi^0$ is an excellent candidate for the discovery of A^0 and at least one of the other two neutral Higgses over the whole intermediate range of M_{A^0} for large values of $\tan\beta$, through the same decay channel $\Phi^0 \rightarrow b\bar{b}$. With respect to charged Higgses, for low(high) values of M_{H^\pm} the dominant production mechanism is $gg \rightarrow t\bar{t} \rightarrow H^+H^-b\bar{b}$ ($bg \rightarrow tH^-$). Because of QCD backgrounds, only the low mass case gives a detectable signal over a non-negligible region of $(M_{A^0}, \tan\beta)$ [20].

At NLC energies, other than via bremsstrahlung and neutral pair production (this latter for H^0A^0 final states too [16]), \mathcal{MSSM} Higgses can be produced also via the fusion processes $e^+e^- \rightarrow \bar{\nu}_e\nu_e W^\pm W^\mp (e^+e^- Z^{0*}Z^{0*}) \rightarrow \bar{\nu}_e\nu_e (e^+e^-)h^0/H^0$ [21] and the charged pair production $e^+e^- \rightarrow \gamma^*, Z^{0*} \rightarrow H^+H^-$ [22]. The lightest \mathcal{CP} -even Higgs h^0 can be detected over the whole \mathcal{MSSM} parameter space, independently of the top and *squark* masses. Therefore, if the h^0 will not be found at the NLC, the \mathcal{MSSM} is ruled out. If the H^0 and A^0 boson masses are less than $\approx 230 \text{ GeV}$, there exists a very large area in the parameter space where all neutral Higgses can be contemporaneously detected for $\sqrt{s_{ee}} = 500 \text{ GeV}$ [23]. A charged Higgs with $M_{H^\pm} < m_b + m_t$ mainly decays to $\nu_\tau\tau^+$ ($\bar{\nu}_\tau\tau^-$) and $c\bar{s}$ ($\bar{c}s$) pairs (with the leptonic mode dominating for $\tan\beta > 1$). If kinematically allowed, a heavy H^\pm decays via the top mode $H^\pm \rightarrow t\bar{b}$ ($t\bar{b}$) (and in some part of the parameter space also to $W^\pm h^0$). In both cases the signature is a cascade with a τ or a b in the final state: therefore, an extremely good mass resolution is crucial in order to reduce the backgrounds from top and boson pair production. For an intermediate H^\pm , if $\tan\beta > 1$, a possible signature is an apparent breaking of the τ vs μ/e universality. At higher e^+e^- energies, such as $\sqrt{s_{ee}} = 1-2 \text{ TeV}$, fusion mechanisms become dominant over other production processes [15, 24].

The conversion of e^+e^- NLCs into $\gamma\gamma$ and/or $e\gamma$ colliders, by photons generated via Compton back-scattering of laser light, provides new possibilities of detecting and studying Higgs bosons [25]. For the \mathcal{MSSM} , at a NLC with $\sqrt{s_{ee}} = 500 \text{ GeV}$, $\gamma\gamma \rightarrow \Phi^0$ reactions are important in searching for heavy H^0 and A^0 bosons: they can be detected up to mass values of $\approx 0.8\sqrt{s_{ee}}$, for moderate $\tan\beta$ and if a luminosity of 20 fb^{-1} , or more, can be achieved

⁶For the *stop* mass $m_{\bar{t}} = 1 \text{ TeV}$ and all ν masses greater than 200 GeV .

⁷If the higher luminosity and a large number of tracks per event can successfully be dealt with.

[26]. For the H^0 , the channels $H^0 \rightarrow h^0 h^0$, if $M_{H^0} \lesssim 2m_t$, and $H^0 \rightarrow t\bar{t}$, for $M_{H^0} \gtrsim 2m_t$, appear more interesting than the decays $H^0 \rightarrow b\bar{b}$ and $H^0 \rightarrow Z^0 Z^0$. For the A^0 , the feasible reactions are $\gamma\gamma \rightarrow A^0 \rightarrow Z^0 h^0 / b\bar{b}$, if $M_{A^0} \lesssim 2m_t$, and $\gamma\gamma \rightarrow A^0 \rightarrow t\bar{t}$, if $M_{A^0} \gtrsim 2m_t$. If $\tan\beta \lesssim 20$, only the $b\bar{b}$ channel is useful for the A^0 , with $M_{A^0} \lesssim 250$ GeV⁸. Recently, it has been shown that the intermediate mass H^+H^- pair production via $\gamma\gamma$ fusion is greater (e.g., at least by a factor 2 at $\sqrt{s_{ee}} = 500$ GeV) than the corresponding e^+e^- mode, and charged Higgses can be detected using the three decay modes $\nu_\tau\tau^+\bar{\nu}_\tau\tau^-$, $c\bar{s}\bar{c}s$ and $c\bar{s}\bar{\nu}_\tau\tau^- + \nu_\tau\tau^+\bar{c}s$ in a complementary way in order to cover all the intermediate mass region of H^\pm [27]. The $e\gamma$ option at NLCs is quite interesting in studying \mathcal{MSSM} Higgs boson production via the processes $e^-\gamma \rightarrow \nu_e W^-\Phi^0$, $e^-\gamma \rightarrow \nu_e H^-\Phi^0$ and $e^-\gamma \rightarrow e^-H^+H^-$, in the intermediate mass range of M_{A^0} and for a large choice of $\tan\beta$'s [28].

The option of ep colliders in detecting and studying \mathcal{MSSM} Higgs bosons has been only marginally exploited, so far, with respect to the possibilities of pp and e^+e^- accelerators. The only presently operating ep high energy machine is HERA [29], which, however, has been primarily designed for providing accurate data on the proton structure functions in the small- x region, more than being devoted to Higgs searches, which are almost impossible even for the more favourable cases of A^0 - and H^\pm -production [30]. In fact, most of these searches rely on very special conditions, which seem to be excluded by recent limits on Higgs and top masses: e.g., very high $\tan\beta$ (≈ 40) in order to detect neutral Higgses Φ^0 via $Z^0 Z^0$ - and $\gamma\gamma$ -fusion processes [31], or very light charged Higgses and/or top quark for H^\pm -production via $\gamma\gamma$ - [32] and γg -fusion [33]. Furthermore, the H^\pm -production mechanism via bremsstrahlung off heavy quarks $\gamma q \rightarrow q'H^\pm$ suffers from a strong Cabibbo-Kobayashi-Maskawa or $\mathcal{O}(\frac{m_q}{M_{W^\pm}})$ suppression (where q is the emitting initial light quark) [34]. Finally, the production of neutral \mathcal{MSSM} Higgses through bremsstrahlung off b -quarks, exploited in ref. [35], can hardly be useful, since it depends not only on a good b - and/or heavy lepton-tagging, but also on the fact that only large $\tan\beta$ (≈ 20) and Higgs masses $M_{\Phi^0} \lesssim 90$ GeV can give detectable signals⁹.

In the future, another ep collider is contemplated to be operating, the CERN LEP \otimes LHC machine, obtainable by combining an electron/positron beam of LEP II and a proton beam of the LHC [9, 36]. The detailed studies on the detectability of an intermediate mass \mathcal{SM} Higgs boson ϕ at such a machine presented in ref. [37] (using $W^\pm W^\mp$ - and $Z^0 Z^0$ -fusion processes [34, 30, 38, 39], with ϕ decaying to $b\bar{b}$) can be transposed to the case of \mathcal{CP} -even neutral \mathcal{MSSM} Higgs bosons, but increasing the requirements on luminosity and/or on b -tagging identification, due to the smaller H^0 and h^0 cross sections with respect to the \mathcal{SM} case. Charged Higgs bosons can be detected at LEP \otimes LHC energies via the decay $t(\bar{t}) \rightarrow H^\pm b(H^\mp\bar{b})$, if $M_{H^\pm} \lesssim m_t - m_b$, while for $M_{H^\pm} \gtrsim m_t - m_b$, good sources of H^\pm bosons are the photo-production $\gamma b \rightarrow H^- t$ (through bremsstrahlung photons) and the W^\pm -mediated process $e^- b \rightarrow \nu_e H^- b$, studied in ref. [40].

Concerning photon-initiated processes, only recently has the possibility of resorting to back-scattered laser γ 's, also at the CERN ep collider, [41] been suggested. This option has been applied to the case of \mathcal{SM} Higgs production but, obviously, it could turn out to be

⁸Since the h^0 mass never becomes large, the only important channel is $\gamma\gamma \rightarrow h^0 \rightarrow b\bar{b}$, allowing its detection for $M_{h^0} \gtrsim 60$ GeV ($M_{A^0} \gtrsim 70$ GeV).

⁹Region that can be more easily covered by LEP II.

useful for \mathcal{MSSM} Higgs bosons also.

It is the purpose of this paper to study at the LEP \otimes LHC ep collider the reactions

$$q\gamma \rightarrow q'W^\pm\Phi^0, \quad (2)$$

$$q\gamma \rightarrow qZ^0\Phi^0, \quad (3)$$

$$q\gamma \rightarrow q'H^\pm\Phi^0, \quad (4)$$

$$q\gamma \rightarrow q\Phi^0\Phi^{0'}, \quad (5)$$

$$q\gamma \rightarrow qH^+H^-, \quad (6)$$

$$g\gamma \rightarrow q\bar{q}'H^\pm, \quad (7)$$

$$g\gamma \rightarrow q\bar{q}\Phi^0, \quad (8)$$

where $\Phi^{0(\prime)} = H^0, h^0$ and A^0 , in the intermediate mass range of A^0 , for all possible (anti)flavours of the (anti)quarks $q(q')$, using laser back-scattered photons. We discuss their relevance for the detection of the \mathcal{MSSM} Higgs bosons and the study of their parameters, assuming b -tagging identification.

We did not study the processes

$$q\gamma \rightarrow qW^\pm H^\mp, \quad (9)$$

$$q\gamma \rightarrow q'Z^0 H^\pm, \quad (10)$$

since here the \mathcal{MSSM} Higgs bosons directly couple to the quark line in each Feynman diagram at tree-level, so we expect that they are suppressed through the Yukawa coupling by the hadron structure functions, with respect to processes (2)–(8), where Φ^0 and H^\pm also couple to the vector bosons γ , Z^0 and W^\pm (see diagrams (7), (8), (13), (14) of fig. 1 and diagrams (7), (8), and (15)–(17) of fig. 2).

There are at least two important motivations for studying processes (2)–(8), and at the LEP \otimes LHC collider. First, the CERN ep option could be operating before any NLC, so it would constitute the first TeV energy environment partially free from the enormous background arising from QCD processes (typical of the purely hadron colliders), which prevents the possibility of detailed studies of the various parameters of an intermediate mass Higgs boson. Second, even in the case that LEP II and LHC can together cover all the parameter space $(M_{A^0}, \tan\beta)$, nevertheless, processes (2)–(8) offer the opportunity for studying a large variety of \mathcal{MSSM} interactions involving Higgs bosons: in fact, all the vertices displayed in tabs. A.I–A.IV occur. Moreover, the additional heavy particles $t(\bar{t})$, W^\pm , Z^0 and the second Higgs boson can be used for tagging purposes, increasing the signal versus background ratio.

The plan of the paper is as follows. In Section II we give some details of the calculation and the numerical values adopted for the various parameters. Section III is devoted to the presentation of the results while the Conclusions are in Section IV. Finally, in the Appendix, we give the tree-level helicity amplitudes for processes (2)–(8).

Calculation

In the unitary gauge the Feynman diagrams which enter in describing reactions (2)–(8) at tree-level are shown in figs. 1, 2 and 3. For the various possible combinations of $(q, q', V, V^*, S^*, \Phi^0)$ in fig. 1, $(q, q', V^*, S^*, S^*, \Phi, \Phi')$ in fig. 2, and (q, q', S^*, Φ) in fig. 3, see details in the Appendix. All quarks have been considered massive, so diagrams with a direct coupling of Φ^0/H^\pm to fermion lines have been computed for each combination of flavours.

The matrix elements have been evaluated by means of the spinor techniques of refs. [42, 43] and the FORTRAN codes have been compared with the corresponding ones implemented by the method of ref. [44]. The amplitudes have been tested for gauge invariance, and it has been also verified that, with appropriate couplings, hadronic distributions and luminosity function of photons, our results for the processes $q\gamma \rightarrow q'W^\pm\Phi^0$, $g\gamma \rightarrow q\bar{q}\Phi^0$ and $g\gamma \rightarrow t\bar{b}H^-$ reproduce those of ref. [41] (for a \mathcal{SM} Higgs), of ref.[35] and of ref. [33], respectively. Furthermore, since a simple adaptation of the formulae given in the Appendix (by changing photon couplings from quarks into leptons and setting the quark masses equal to zero) allows us to reproduce the computations of ref. [28], we have checked, where possible, our helicity amplitudes also in these limits.

As proton structure functions we adopted the recent set MRS(A) [45], fixing the μ -scale equal to the Center of Mass energy (CM) at parton level (i.e., $\mu = \sqrt{\hat{s}_{q(g)\gamma}}$). The strong coupling constant α_s , which appears in the gluon initiated processes, has been evaluated at next-to-leading order, with $\Lambda_{\overline{MS}}^4 = 230$ MeV and a scale μ equal to the one used for the proton structure functions, and consistent with the quark flavour entering in the partonic subprocess. We are confident that changing the energy scale and/or the distribution functions choice should not affect our results by more than a factor of two.

For the energy spectrum of the back-scattered (unpolarized) photon we have used [46]

$$F_{\gamma/e}(x) = \frac{1}{D(\xi)} \left[1 - x + \frac{1}{1-x} - \frac{4x}{\xi(1-x)} + \frac{4x^2}{\xi^2(1-x)^2} \right], \quad (11)$$

where $D(\xi)$ is the normalisation factor

$$D(\xi) = \left(1 - \frac{4}{\xi} - \frac{8}{\xi^2} \right) \ln(1 + \xi) + \frac{1}{2} + \frac{8}{\xi} - \frac{1}{2(1 + \xi)^2}, \quad (12)$$

and $\xi = 4E_0\omega_0/m_e^2$, where ω_0 is the incoming laser photon energy and E_0 the (unpolarized) electron/positron one. In eq. (11), $x = \omega/E_0$ is the fraction of the energy of the incident electron/positron carried by the back-scattered photon, with a maximum value

$$x_{\max} = \frac{\xi}{1 + \xi}. \quad (13)$$

In order to maximise ω while avoiding e^+e^- pair creation, one takes ω_0 such that $\xi = 2(1 + \sqrt{2})$. So, in the end, one gets the typical values $\xi \simeq 4.8$, $x_{\max} \simeq 0.83$, $D(\xi) \simeq 1.8$.

In the case of $q(g)\gamma$ scatterings from ep collisions, the total cross section σ is obtained by folding the subprocess cross section $\hat{\sigma}$ with the photon $F_{\gamma/e}$ and hadron $H_{q(g)/p}$ luminosities:

$$\sigma(s_{ep}) = \int_{x_{\min}^\gamma}^{x_{\max}^\gamma} dx^\gamma \int_{x_{\min}^{q(g)}}^{1-x^\gamma} dx^{q(g)} F_{\gamma/e}(x^\gamma) H_{q(g)/p}(x^{q(g)}) \hat{\sigma}(\hat{s}_{q(g)\gamma} = x^\gamma x^{q(g)} s_{ep}), \quad (14)$$

where $\hat{s}_{q(g)\gamma}$ is the CM energy at parton (i.e., $q(g)\gamma$) level, while

$$x_{\min}^\gamma x_{\min}^{q(g)} = \frac{(M_{\text{final}})^2}{s_{ep}}, \quad (15)$$

with M_{final} the sum of the final state particle masses.

The total cross section has been then obtained numerically integrating over the phase space using the Monte Carlo routine VEGAS [47].

So far, to our knowledge, a detailed study, like in the case of $e\gamma$ and $\gamma\gamma$ collisions [46], on the efficiency of the laser back-scattering method in converting $e \rightarrow \gamma$ at ep colliders does not exist. In this work we assume the effective γp luminosity to be equal to the ep one (see ref. [48]). For the discussion of the results we have assumed an overall total integrated luminosity $\mathcal{L} = 3 \text{ fb}^{-1}$, according to value adopted in ref. [41].

Within the $MSSM$, in order to simplify the discussion, we assume an universal soft supersymmetry-breaking mass [49, 50]

$$m_Q^2 = m_U^2 = m_D^2 = m_{\tilde{q}}^2, \quad (16)$$

and a negligible mixing in the *stop* and *sbottom* mass matrices

$$A_t = A_b = \mu = 0. \quad (17)$$

If we also neglect the *bottom* mass in the formulae of refs. [49, 50], the one-loop corrected masses of the $MSSM$ neutral \mathcal{CP} -even Higgs bosons can be expressed in terms of a single parameter ϵ [51], given by

$$\epsilon = \frac{3e^2}{8\pi^2 M_{W^\pm}^2 \sin^2 \theta_W} m_t^4 \ln \left(1 + \frac{m_{\tilde{q}}^2}{m_t^2} \right). \quad (18)$$

Diagonalization of the mass squared matrix leads to the expressions¹⁰

$$\begin{aligned} M_{h^0, H^0}^2 &= \frac{1}{2} [M_{A^0}^2 + M_{Z^0}^2 + \epsilon/s_\beta^2] \\ &\pm \left\{ [(M_{A^0}^2 - M_{Z^0}^2)c_{2\beta} + \epsilon/s_\beta^2]^2 + (M_{A^0}^2 + M_{Z^0}^2)^2 s_{2\beta}^2 \right\}^{1/2}, \end{aligned} \quad (19)$$

while the mixing angle α in the \mathcal{CP} -even sector is defined at one-loop by

$$t_{2\alpha} = \frac{(M_{A^0}^2 + M_{Z^0}^2)s_{2\beta}}{(M_{A^0}^2 - M_{Z^0}^2)c_{2\beta} + \epsilon/s_\beta^2}, \quad -\frac{\pi}{2} < \alpha \leq 0. \quad (20)$$

For the $MSSM$ charged Higgs masses we have maintained the tree-level relations

$$M_{H^\pm}^2 = M_{A^0}^2 + M_{W^\pm}^2, \quad (21)$$

since the one-loop corrections are quite small if compared with the corresponding ones for neutral Higgses [50].

¹⁰Throughout this paper we use the notations $s_x = \sin(x)$, $c_x = \cos(x)$, $t_x = \tan(x)$ (with $x = \alpha, \beta, 2\alpha$ and 2β), $s_{\alpha\beta} = \sin(\beta + \alpha)$, $c_{\alpha\beta} = \cos(\beta + \alpha)$, $s_{\beta\alpha} = \sin(\beta - \alpha)$ and $c_{\beta\alpha} = \cos(\beta - \alpha)$.

Concerning the numerical part of our work, we have adopted $\alpha_{em} = 1/128$ and $\sin^2 \theta_W \equiv s_W^2 = 0.23$, for the e.m. coupling constant and the sine squared of the Weinberg angle, respectively. For the gauge boson masses and widths we have taken: $M_{Z^0} = 91.175$ GeV, $\Gamma_{Z^0} = 2.5$ GeV, $M_{W^\pm} = M_{Z^0} \cos \theta_W \equiv M_{Z^0} c_W \approx 80$ GeV and $\Gamma_{W^\pm} = 2.2$ GeV; while for the fermion masses: $m_e = 0.511 \times 10^{-3}$ GeV, $m_\mu = 0.105$ GeV, $m_\tau = 1.78$ GeV, $m_u = 8.0 \times 10^{-3}$ GeV, $m_d = 15.0 \times 10^{-3}$ GeV, $m_s = 0.3$ GeV, $m_c = 1.7$ GeV, $m_b = 5.0$ GeV and, e.g., according to the CDF announcement [52], $m_t = 175$ GeV, with all widths equal to zero except the top one, which has been computed at tree-level within the \mathcal{MSSM} , using the expressions [53]:

$$\frac{\Gamma(t \rightarrow bH^+)}{\Gamma(t \rightarrow bW^+)} = \frac{\lambda(M_{H^\pm}^2, m_b^2, m_t^2)^{1/2}}{\lambda(M_{W^\pm}^2, m_b^2, m_t^2)^{1/2}} \times \frac{(m_t^2 + m_b^2 - M_{H^\pm}^2)(m_t^2 t_\beta^{-2} + m_b^2 t_\beta^2) + 4m_t^2 m_b^2}{M_{W^\pm}^2 (m_t^2 + m_b^2 - 2M_{W^\pm}^2) + (m_t^2 - m_b^2)^2}, \quad (22)$$

and [54]

$$\Gamma(t \rightarrow bW^+) = |V_{tb}|^2 \frac{G_F m_t}{8\sqrt{2}\pi} \lambda(M_{W^\pm}^2, m_b^2, m_t^2)^{1/2} \times \left\{ \left[1 - \left(\frac{m_b}{m_t}\right)^2\right]^2 + \left[1 + \left(\frac{m_b}{m_t}\right)^2\right] \left(\frac{M_{W^\pm}}{m_t}\right)^2 - 2\left(\frac{M_{W^\pm}}{m_t}\right)^4 \right\}, \quad (23)$$

where V_{tb} is the Cabibbo–Kobayashi–Maskawa mixing term (here set equal to 1), $G_F = \sqrt{2}g^2/8M_{W^\pm}^2$ the electroweak Fermi constant, $g = e/s_W$ with $-e$ the electron charge, and $\lambda^{1/2}$ the usual kinematic factor

$$\lambda(M_a, M_b, M_c)^{1/2} = [M_a^2 + M_b^2 + M_c^2 - 2M_a M_b - 2M_a M_c - 2M_b M_c]^{1/2}. \quad (24)$$

All neutrino's have been considered massless: i.e., $m_{\nu_e} = m_{\nu_\mu} = m_{\nu_\tau} = 0$, with null corresponding widths.

The widths of the \mathcal{MSSM} Higgs bosons have been evaluated for the same \mathcal{MSSM} parameters we adopted in the cross section analysis: for the numerical values as for further details on their computation we refer to [55].

Finally, the universal supersymmetry–breaking squark mass has been fixed in the numerical analysis to the value $m_{\bar{q}} = 1$ TeV, and at the same time, for simplicity, we have ignored the presence of not–Higgs supersymmetric particles (i.e., squarks, sleptons, gauginos, higgsinos).

We have analysed processes (2)–(8) in the mass range 60 GeV $\lesssim M_{A^0} \lesssim 140$ GeV, with $\tan\beta = 1.5, 30$, at the ep CM energy $\sqrt{s_{ep}} = 1.36$ TeV.

Results

As it is unpractical to cover all regions of the \mathcal{MSSM} parameter space ($M_{A^0}, \tan\beta$) (for intermediate masses of the pseudoscalar Higgs boson), we have chosen here, as representative for $\tan\beta$, the two extreme values 1.5 and 30, whereas M_{A^0} spans in the range 60 to 140 GeV. Also, due to the huge amount of computing time that otherwise would have been necessary,

and contrary to the \mathcal{SM} analysis of ref. [48], we concentrate here only on the energy of the proposed CERN ep collider ($\sqrt{s}_{ep} = 1.36$ TeV) [9]. At this CM energy the cross sections (summed over all possible flavour combinations) for the processes:

$$q\gamma \rightarrow q'W^\pm\Phi^0, \quad \Phi^0 = H^0, h^0, A^0, \quad (25)$$

$$q\gamma \rightarrow qZ^0\Phi^0, \quad \Phi^0 = H^0, h^0, A^0, \quad (26)$$

$$q\gamma \rightarrow q'H^\pm\Phi^0, \quad \Phi^0 = H^0, h^0, A^0, \quad (27)$$

$$q\gamma \rightarrow q\Phi^0\Phi^{0'}, \quad (\Phi^0, \Phi^{0'}) = (H^0, A^0), (h^0, A^0), \quad (28)$$

$$q\gamma \rightarrow qH^+H^-, \quad (29)$$

$$g\gamma \rightarrow q\bar{q}'H^\pm, \quad (30)$$

$$g\gamma \rightarrow q\bar{q}\Phi^0, \quad \Phi^0 = H^0, h^0, A^0, \quad (31)$$

are given in tabs. Ia–VIIb. Since the production rates for the reactions

$$q\gamma \rightarrow q\Phi^0\Phi^{0'}, \quad (\Phi^0, \Phi^{0'}) = (H^0, H^0), (H^0, h^0), (h^0, h^0), (A^0, A^0), \quad (32)$$

are generally¹¹ never larger than $\mathcal{O}(10^{-2})$ fb and are beyond any experimental possibility of detection, we do not give their rates here and we will not consider them in the forthcoming analysis either¹². Before proceeding further, a few comments are in order now, concerning the characteristics of the signals.

Process (25) gives quite large rates for the case $\Phi^0 = H^0$ and not too large values of M_{A^0} ($\lesssim 120$ GeV), both for $\tan\beta = 1.5$ and $\tan\beta = 30$, with the cross sections corresponding to the last case being larger. Significantly large numbers occur also in the case $\Phi^0 = h^0$, more at small than at large $\tan\beta$'s. Phase space effects due to the increase of M_{H^0} and M_{h^0} lower down the cross sections, whereas the strong change of trend at large $\tan\beta$'s and $M_{A^0} \approx 120 - 140$ GeV is due to the sudden step decrease of the $H^0W^+W^-$ coupling (proportional to $c_{\beta\alpha}$), and to the corresponding increase of the $h^0W^+W^-$ one (proportional to $s_{\beta\alpha}$). Higgs bremsstrahlungs diagrams (numbers 1–6 in fig. 1) are in fact drastically suppressed because of the Yukawa coupling $\Phi^0q\bar{q}$, proportional to m_q , since q (due to the partonic distributions) is most of the times a light quark. Because of this, and since the A^0 does not couple at tree-level to the W^\pm 's, the case $\Phi^0 = A^0$ generally gives much smaller rates. Only the case $\tan\beta = 30$ (i.e., large $\Phi^0D\bar{D}$ coupling to down-type quarks D), for small enough phase space suppression (i.e., if $M_{A^0} \approx 60$ GeV), can give cross sections of $\mathcal{O}(1)$ fb.

Same considerations as the above mentioned apply to the case of reaction (26), even though the suppressed $\Phi^0Z^0Z^0$ couplings (with respect to the case $\Phi^0W^+W^-$, being $\Phi^0 = H^0, h^0$) yield contributions which are in general an order of magnitude smaller than in the previous case. At $\tan\beta = 1.5$ only the h^0 seems to be interesting, whereas at $\tan\beta = 30$

¹¹Apart from the cases (h^0, h^0) and (A^0, A^0) for $M_{A^0} = 60 - 80$ GeV, with $\tan\beta = 1.5, 30$ and 30 , respectively, which can reach cross sections of $\mathcal{O}(1)$ fb.

¹²Also, in some instances, results given in tabs. Ia–VIIb will be very small. Nevertheless, we present them with the purpose of comparison, in order to facilitate the discussion in terms of dependence on masses, couplings, etc ...

both the H^0 and the h^0 show negligible numbers. Finally, graphs with Higgs-strahlungs off b -quarks contribute to keep the rates for the A^0 at $\tan\beta = 30$ at the level of $\mathcal{O}(1)$ fb, if M_{A^0} is not too large, whereas at $\tan\beta = 1.5$ numbers are completely negligible.

The coupling of the A^0 to the vertices $\Phi^0 W^\pm H^\mp(\gamma)$ (see tab. A.I in the appendix) does not suffer from angular factor suppression (there is no dependence on α and β), whereas H^0 's and h^0 's do. Therefore, the rates for the A^0 in the case of reaction (27) are larger than the ones of the CP -even scalars, both a $\tan\beta = 1.5$ and $\tan\beta = 30$. This latter observation is always true apart from the case $\tan\beta = 30$ and $M_{A^0} \lesssim 120$ GeV, where numbers for the pseudoscalar and the light scalar are practically the same, as the value of $c_{\beta\alpha}$ approaches 1. This also proves that diagrams with $\Phi^0 H^+ H^-$ couplings (graphs 13–14 in fig. 2, which are zero for $\Phi^0 = A^0$) do not count. The same can be affirmed for neutral Higgs bremsstrahlung diagrams, because they always occur in conjunction with a $H^\pm q\bar{q}'$ Yukawa coupling (see the practically unchanged rates for the A^0 at both values of $\tan\beta$).

The case $(\Phi^0, \Phi^{0'}) = (H^0, A^0)$ in process (28) is never interesting (and it has been shown for comparison purposes only, against the combination $h^0 A^0$). Due to the double Yukawa coupling, diagrams 1–6 in fig. 2 essentially never enter. Diagrams 9–10 are strongly suppressed at $\tan\beta = 1.5$, whereas at $\tan\beta = 30$ they give a small contribution (because of the $A^0 D\bar{D}$ vertex). However, the largest rates come from diagrams 7–8, which are proportional to $s_{\beta\alpha}^2$ and $c_{\beta\alpha}^2$, for the H^0 and the h^0 , respectively. As the second coupling is larger than the first one and $M_{H^0} > M_{h^0}$ in our range of interest, it is clear that H^0 rates are again smaller compared to the h^0 ones (especially at $\tan\beta = 30$).

Process (29) is one of those for which the production rates are bigger, if M_{A^0} is not too large. The major partonic contributions here come from the subprocess with resonant top-quarks (i.e., $b\gamma \rightarrow bH^+H^-$). Diagrams with $\gamma^*(Z^{0*})H^+H^-$ couplings (i.e., with a virtual photon or Z^0 splitting into H^+H^- -pairs) are dominant only in the other cases (for $q = u, d, s, c$). The increase of the rates with $\tan\beta$ is due to the larger contribution of graphs 8–10 and 13–14, which involve $\Phi^0 D\bar{D}$ couplings ($\Phi^0 = H^0$ and h^0).

For process (30), practically, the whole of the partonic contribution comes from the combination $g\gamma \rightarrow t\bar{b}H^+ + \text{c.c.}$, because of the bt Yukawa couplings of the H^\pm and because of the top resonance. Therefore, the increase of the rates with the increase of $\tan\beta$ in tabs. VIa–b exclusively depends on and can be understood in terms of the coupling $H^\pm t\bar{b}$. Graphs with γH^+H^- vertices are generally suppressed in the $t\bar{b}H^\pm$ case, and phase space effects act in such a way to strongly reduce the rates for increasing M_{A^0} (because of the quite large value of m_t).

In case of process (31) we can greatly appreciate the benefits of $\Phi^0 D\bar{D}$ Yukawa couplings with large $\tan\beta$: in fact, all the flavours $\Phi^0 = H^0, h^0$ and A^0 have large cross sections at $\tan\beta = 30$. This happens especially for the pseudoscalar (it has a $\sim \tan\beta$ quark-coupling) and the light scalar ($\sim s_\alpha/c_\beta$ quark-coupling). The decrease of their rates with an increasing M_{A^0} is due to a phase space effect in the former case, whereas in the latter also a reduction due to the diminishing of s_α occurs. Since the H^0 quark-coupling is proportional to c_α/c_β , in this case things proceed the other way round. In addition, the suppression due to phase space effects is small here, as M_{H^0} varies by only ≈ 10 GeV in the usual M_{A^0} range, if $\tan\beta = 30$. At $\tan\beta = 1.5$ rates are generally much smaller, being noticeable only for h^0 (small mass and large s_α).

The main lines of the analysis we will perform in order to select the signal events out of the backgrounds are the same ones already adopted for the \mathcal{SM} case, in ref. [48]. In order to maximise the event rates, we will consider the decay channels with highest Branching Ratio (BR). Therefore, we will look for the Higgs decay channel $\Phi^0 \rightarrow b\bar{b}$ for the neutral Higgs flavours h^0 , A^0 and H^0 , whereas, in case of charged Higgses, we will concentrate on the decay $H^\pm \rightarrow \tau\nu_\tau$. We know that for $\tan\beta = 1.5(30)$ and $60 \text{ GeV} \leq M_{A^0} \leq 140 \text{ GeV}$ ($M_{A^0} \approx 60 \text{ GeV}$), corresponding to $145 \text{ GeV} \lesssim M_{H^0} \lesssim 180 \text{ GeV}$ ($M_{H^0} \approx 129 \text{ GeV}$), the BRs of the decay channels $H^0 \rightarrow W^{+*}W^{-*}$ ($H^0 \rightarrow W^{+*}W^{-*}$) and, for $M_{H^0} \lesssim 150 \text{ GeV}$, $H^0 \rightarrow h^0h^0$ ($H^0 \rightarrow h^0h^0$ and $H^0 \rightarrow A^0A^0$), are larger than $\text{BR}(H^0 \rightarrow b\bar{b})$ [55]. Nevertheless, we concentrate here on the last decay only, for various reasons. In the case of $W^{+*}W^{-*}$ -decays, we should first add, in any case, an additional reduction factor due to the $W^{\pm*}$ -decay channels (that we should, in some how, identify). Second, we would end up considering signatures of the type $jj(Y)$, $(\tau\nu_\tau)(Y)$ or $(b\bar{b})(Y)$ (see later on), where $Y = 4j, 2j2\ell$, or 4ℓ , with the clear disadvantages of dealing either with a large number of jets (for $Y = 4j, 2j\ell\nu_\ell$, which would have both a large QCD and combinatorial background) or with missing energy/momenta (for $Y = \ell\nu_\ell\ell\nu_\ell$, which would prevent from reconstructing Higgs peaks by means of invariant mass spectra). In the case of h^0h^0 - and A^0A^0 -decays, in order to keep high rates, we should consider the channels $h^0h^0, A^0A^0 \rightarrow 4b$, which would lead to the difficult requirement of recognising with high efficiency at least four b 's in a single event. Whereas the decay $H^0 \rightarrow b\bar{b}$ implies that the only reduction factor is the $b\bar{b}$ -BR, which ranges in the above interval of M_{H^0} , for $\tan\beta = 1.5(30)$, between $\approx 4(3)$ and $\approx 20(90)\%$ [55]. In the case of charged Higgs decays, if $\tan\beta = 1.5$ and $M_{H^\pm} \gtrsim 150 \text{ GeV}$, the tb channel has a BR larger than the one into $\tau\nu_\tau$ -pairs. However, as $\text{BR}(H^\pm \rightarrow tb)$ is not too drastically larger (so the loss of statistics is not substantial) and the decay chain $H^\pm \rightarrow tb \rightarrow b\bar{b}W^\pm + b\bar{b}H^\pm$ would lead to a more complicated final state with additional backgrounds, for the moment, we consider the $H^\pm \rightarrow \tau\nu_\tau$ channel only.

We will require hadronic decays of the massive vectors bosons (W^\pm and Z^0) and, in order to select the $b\bar{b}$ Higgs decay out of the QCD background, we will assume excellent flavour identification of b -quarks [56], such that we can get rid of the non- b multi-jet photoproduction, $W^\pm + \text{jets}$ and $Z^0 + \text{jets}$ background events [41], and that a $M_{b\bar{b}}$ cut around the Φ^0 masses (see later on) is sufficient in order to suppress the above processes in the case of $\gamma^*/g^* \rightarrow b\bar{b}$ splitting.

Therefore, we expect the following signatures:

$$q'W^\pm\Phi^0 \rightarrow (jj)(b\bar{b})X, \quad (33)$$

$$qZ^0\Phi^0 \rightarrow (jj)(b\bar{b})X, \quad (34)$$

$$q'H^\pm\Phi^0 \rightarrow (\tau\nu_\tau)(b\bar{b})X, \quad (35)$$

$$qH^0A^0, qh^0A^0 \rightarrow (b\bar{b})(b\bar{b})X, \quad (36)$$

$$qH^+H^- \rightarrow (\tau\nu_\tau)(\tau\nu_\tau)X, \quad (37)$$

$$q\bar{q}'H^\pm \rightarrow jj(\tau\nu_\tau)X \text{ (if } q\bar{q}' \neq t\bar{b}) \text{ or } t\bar{b}(\tau\nu_\tau)X \rightarrow b\bar{b}(\tau\nu_\tau)X \text{ (if } q\bar{q}' = t\bar{b}), \quad (38)$$

$$q\bar{q}\Phi^0 \rightarrow (jj)(b\bar{b})X \text{ (if } q \neq b, t) \text{ or } (b\bar{b})(b\bar{b})X \text{ (if } q = b, t), \quad (39)$$

where X represents the untagged particles in the final states.

Concerning the expected backgrounds¹³ to the above signatures, in case of neutral scalar production (i.e., eqs. (33)–(36) and (39)) we have to consider the same processes already analysed in ref. [48] for the \mathcal{SM} : i.e., $ep \rightarrow W^\pm Z^0 X$, $ep \rightarrow \bar{t}bX \rightarrow \bar{b}\bar{b}W^- X$, $ep \rightarrow t\bar{t}X \rightarrow \bar{b}\bar{b}W^\pm X$, $ep \rightarrow Z^0 Z^0 X$ and $ep \rightarrow q\bar{q}Z^0$. In the case of double and single charged scalar production (i.e., eqs. (37)–(38), respectively), we must add the reactions $ep \rightarrow W^+W^- X$ and $ep \rightarrow tbW^\pm X$. We also notice how the process $ep \rightarrow Z^0 Z^0 X$ is a background to H^+H^- -production when $Z^0 Z^0 \rightarrow (\tau^+\tau^-)(\nu_\tau\bar{\nu}_\tau)$ and that the double and single top-resonant backgrounds $t\bar{t}X$ and tbX , as in the \mathcal{MSSM} t -quarks can decay either to bW^\pm - or bH^\pm -pairs, are a potential background for $W^\pm\Phi^0 X \rightarrow W^\pm(\bar{b}b)X$, $H^\pm\Phi^0 X \rightarrow H^\pm(\bar{b}b)X$ and $\bar{t}bH^- + \bar{t}bH^+ \rightarrow \bar{b}\bar{b}H^\pm X$.

In tabs. VIIIa–b we update the results given in [48] for the neutral scalar production backgrounds, as we are using here a more recent set of structure functions (compare to tab. III in ref. [48]), and, at the same time, we give the rates also for the additional cases $ep \rightarrow qW^+W^-$ ($q \neq b$) and $ep \rightarrow q\bar{q}'W^\pm$ ($q\bar{q}' \neq \bar{t}b$). In tab. VIIIa, a sum over all possible combinations of flavours (not involving top resonances) is implied everywhere. In particular, we notice how in the case of the subprocesses $b\gamma \rightarrow W^- Z^0 t + \text{c.c.}$ and $g\gamma \rightarrow t\bar{t}Z^0$ there are top quarks involved as well: however, as they are produced on-shell in our computations, they do not have any dependence on the \mathcal{MSSM} parameters. On the contrary, in the case of the top resonant backgrounds tbX , $t\bar{t}X$, $W^+W^- X$ (via b -initiated subprocesses) and $q\bar{q}'W^\pm X$ (for $q\bar{q}' = \bar{t}b + \text{c.c.}$) there is such a dependence. Since $\Gamma_t^{\mathcal{MSSM}}$ is function of M_{H^\pm} and $\tan\beta$ (at tree-level), ten different cross sections appear in tab. VIIIb. The total top width in the \mathcal{MSSM} (together with the BRs of the top quark into bW^\pm and bH^\pm), for the two values $\tan\beta = 1.5$ and 30, is given in tab. IX.

Also, we would like to stress here a few details concerning the rates for top production via $g\gamma$ -fusion. The case labeled $tbW^\pm X$ corresponds to top production via the two-to-three body subprocess $g\gamma \rightarrow \bar{t}bW^- + \text{c.c.}$ (including all the 8 diagrams at tree-level giving a gauge invariant set), whereas $tbX \rightarrow \bar{b}\bar{b}W^+W^- X$ and $t\bar{t}X \rightarrow \bar{b}\bar{b}W^+W^- X$ correspond to the rates obtained for the subprocesses $g\gamma \rightarrow \bar{b}\bar{b}W^+W^-$ via graphs with one (12 diagrams) or two (2 diagrams) top resonances, respectively. That is, in the case of the two-to-four body process, we considered only the amplitudes squared of two subsets of the complete set of tree-level Feynman graphs, neglecting their interference. This clearly turns out to be an approximation (and not gauge invariant). However, as single and double top production in $g\gamma \rightarrow \bar{b}\bar{b}W^+W^-$ events are by far the dominant contributions we expect to reproduce quite accurately the complete calculation. In order to check the self-consistency of our results, e.g., one can take, on the one hand, the cross section for $\bar{t}bW^- X + \text{c.c.}$ in case of tt - (2 diagrams, yielding, e.g., at $\tan\beta = 1.5$ and $M_{A^0} = 60$ GeV, ≈ 1195 fb) plus the one for single t -production (6 diagrams, with $\sigma \approx 406$ fb, for the same choice of parameters ($M_{A^0}, \tan\beta$) as above) and multiply these by the corresponding BR($t \rightarrow bW^\pm$) within the \mathcal{MSSM} (see tab. IX), after dividing by two the contribution of the tt -resonant part (thus avoiding problems of double counting), and, on the other hand, the sum of the rates in third and fourth column of tab. VIIIb, then he ends up with numbers that are ‘roughly’ the ones within the computational errors of the others. The above approximate procedure has been adopted in order to avoid prohibitive CPU-time consumes in calculating the complete

¹³These have been evaluated with the help of Madgraph/HELAS [57].

$g\gamma \rightarrow b\bar{b}W^+W^-$ process (52 Feynman graphs at tree-level, including Higgs contributions and keeping the W^\pm 's on-shell).

In case of neutral Higgs production, we divide the backgrounds in continuum and discrete. The first are the ones in which the $b\bar{b}$ -pair does not come from a Z^0 -resonance (i.e., $t\bar{b}X$ and $t\bar{t}X$), and the second the ones in which the b 's are the decay products of the Z^0 . Following the above distinction also in the case of double and single H^\pm -production, it turns out that H^\pm -signals have only discrete backgrounds, in which the $\tau\nu_\tau$ -pair comes from a decaying W^\pm .

Although the background rates are in some instances much larger than the corresponding signals, one has to remember that the discrete backgrounds can be potentially dangerous only in the cases $M_{\Phi^0} \approx M_{Z^0}$ and $M_{H^\pm} \approx M_{W^\pm}$, while the continuum ones should have a quite flat distribution in the $M_{b\bar{b}}$ spectrum, where $M_{b\bar{b}}$ is the invariant mass of the $b\bar{b}$ -pair. As the aim of a phenomenological analysis is to finally select signal candidate events in a window around the Breit-Wigner resonance of the Higgs bosons, we will ask that, say, $|M_{\Phi^0(H^\pm)} - M_{b\bar{b}(\tau\nu_\tau)}| < 5 \text{ GeV}$ ¹⁴. If we naively assume that the invariant mass spectra of the discrete backgrounds are all contained in the regions $|M_{Z^0} - M_{b\bar{b}}| \leq 2\Gamma_{Z^0} = 5 \text{ GeV}$ and $|M_{W^\pm} - M_{\tau\nu_\tau}| \leq 2\Gamma_{W^\pm} \approx 5 \text{ GeV}$, then the fraction of Z^0/W^\pm -resonant background events which overlap signal events is given by [58]

$$\delta\sigma(Z^0/W^\pm) = \sigma(Z^0/W^\pm) \frac{\max(0, 10 \text{ GeV} - |M_{\Phi^0/H^\pm} - M_{Z^0/W^\pm}|)}{10 \text{ GeV}}, \quad (40)$$

for $\Phi^0 = H^0, h^0$ and A^0 . In using the above equation we tacitly assumed that also the $\Phi^0 \rightarrow b\bar{b}$ and $H^\pm \rightarrow \tau\nu_\tau$ peaks are all contained in a region of 10 GeV around the Higgs-poles¹⁵.

In addition, in case of continuum backgrounds, as these are top-resonant processes and we are considering hadronic decays of the W^\pm 's, in order to further enhance the signal versus background ratio, we can impose the veto, say, $|M_{bW \rightarrow b(jj)} - m_t| > 15 \text{ GeV}$. Since by the time the LEP⊗LHC collider will be operating the value of the top mass will be well determined, it is quite likely that the above constrain could reveal very efficient.

As criteria for the observability of a signal, we require a rate of $S \geq 6$ events with a significance $S/\sqrt{B} > 4$ for the detection of an isolated Higgs peak, while for the case of Higgs peaks overlapping with Z^0 or W^\pm peaks we require $S \geq 10$ with $S/\sqrt{B} > 6$ [58].

In what follows we will concentrate only on the regions of parameter space $(M_{A^0}, \tan\beta)$ where we have enough rates to presumably make a statistically significant analysis: say, at least $\mathcal{O}(1)$ fb of cross section, and we will analyse the signatures in eqs. (33)–(39) separately.

A. Signature $b\bar{b}b\bar{b}$.

In this case we have contributions from the signals $H^0 A^0 X$, $h^0 A^0 X$ and $q\bar{q}\Phi^0$ (here $q = b, t$, with $t\bar{t}\Phi^0 \rightarrow b\bar{b}\Phi^0 X$, flavours which give the whole of the cross sections in tabs. VIIa–b),

¹⁴We do not repeat here the considerations which induced us to adopt a relatively high mass resolution, as they have been discussed for the case of the \mathcal{SM} analysis. For this, we again refer the reader to ref. [48].

¹⁵In fact, the largest Higgs width in the region of the parameter space here considered happens for the heavy scalar H^0 , at $M_{A^0} = 140 \text{ GeV}$ and for $\tan\beta = 30$, giving $\Gamma_{H^0} \approx 2.9 \text{ GeV}$.

and from the backgrounds $Z^0 Z^0 X$ and $q\bar{q}Z^0 X$, this latter for $q = b, t$, which yields a cross section of ≈ 110 fb.

Here, the most interesting region in the plane $(M_{A^0}, \tan\beta)$ is the one with $\tan\beta = 30$, value for which the combination $h^0 A^0$ seems to be quite promising if $M_{A^0} \approx 60$ GeV (see tab. IVb), whereas the rates for $q\bar{q}\Phi^0$ are very large over all the intermediate spectrum of M_{A^0} , if $\Phi^0 = h^0, A^0$. In the case $q\bar{q}H^0$ rates are small if $M_{A^0} \lesssim 100$ GeV. For $\mathcal{L} = 3 \text{ fb}^{-1}$, after a few years of running, it should be possible to accumulate some tens of $h^0 A^0 X$ events, practically free from backgrounds, as both the A^0 - and h^0 -peaks are quite distant from the Z^0 -one. The combination $H^0 A^0$ is too small for deserving experimental attention, even it doesn't substantially contribute in a possible $A^0 X$ inclusive analysis. The cases $q\bar{q}h^0$ and $q\bar{q}A^0$ give hundreds or thousands of events per year, which should be easily recognised if $M_{h^0}, M_{A^0} \neq M_{Z^0}$. In the case of overlapping Z^0 and h^0/A^0 peaks, Higgs signal could be recognised in the form of an excess of $b\bar{b}$ events at the Z^0 peak. For $q\bar{q}H^0$, as $M_{H^0} - M_{Z^0} \gg 10$ GeV in the range where H^0 -rates are large, there should not be any problem in selecting the signal. The case $\tan\beta = 1.5$ seems to be quite discouraging for all the above signals.

As this signature involves four b -quarks it is crucial that high b -tagging performances can be achieved.

B. Signature $jj\bar{b}\bar{b}$.

This channel receives contributions from the signals $W^\pm\Phi^0 X$ and $Z^0\Phi^0 X$. The case $q\bar{q}\Phi^0$ for light flavours $q = u, d, s$ and c practically does not give any event for all Φ^0 's, as the bulk of the cross sections come from the subprocesses $q\bar{q}\Phi^0$ with $q = b, t$, which give the already considered $4b$ -signature. The backgrounds are $W^\pm Z^0 X$, $Z^0 Z^0 X$, and $q\bar{q}Z^0 X$ for $q \neq b, t$, which yields a cross section of ≈ 3000 fb. In addition, the continuum processes $tbX \rightarrow b\bar{b}W^\pm X$ and $t\bar{t}X \rightarrow b\bar{b}W^\pm X$ enter here as well (with $W^\pm \rightarrow jj$ ¹⁶).

Due to the small rates, we did not consider here A^0 -production at $\tan\beta = 1.5$. Once one multiplies the rates of signal and backgrounds by the BRs giving the signature $jj\bar{b}\bar{b}$, by the yearly luminosity $\mathcal{L} = 3 \text{ fb}^{-1}$ and picks up events in the windows $|M_{b\bar{b}} - M_{\Phi^0}| < 5$ GeV, it comes out that the only case which can give significancies large enough to allow for possible detection is for $\Phi^0 = h^0$ at $\tan\beta = 1.5$. The value of S/\sqrt{B} is approximately 4 over all the range $56 \text{ GeV} \lesssim M_{h^0} \lesssim 81 \text{ GeV}$. The case $\Phi^0 = H^0$ at $\tan\beta = 30$, which has production rates comparable to the ones of the previous case, is overwhelmed by the tbX and $t\bar{t}X$ backgrounds (both productions rates and BRs into $b\bar{b}$ -pairs are in fact smaller with respect to the light neutral Higgs). Therefore, in the channel $jj\bar{b}\bar{b}$ only the h^0 scalar can be detected, and only for large $\tan\beta$'s.

¹⁶It would be worth here to consider also $tbX \rightarrow b\bar{b}H^\pm X$ and $t\bar{t}X \rightarrow b\bar{b}H^\pm X$ as background, although they contain a $MSSM$ charged Higgs. In fact, H^\pm 's can decay to jj -pairs. However, as this channel has a small branching ratio (other than originating from already suppressed $t \rightarrow bH^\pm$ decays, see tab. IX) and as we are tacitly assuming that the two jets in the signature $jj\bar{b}\bar{b}$ reproduce the $W^\pm(Z^0)$ -mass (note that $M_{H^\pm} - M_{W^\pm(Z^0)} \gtrsim 20(10) \text{ GeV}$), we can safely neglect the two above background contributions.

C. Signature $\tau\nu_\tau b\bar{b}$.

In this case, we have to consider $H^\pm\Phi^0 X$, $tbH^\pm \rightarrow b\bar{b}H^\pm X$ as signals, and $W^\pm Z^0 X$ and $tbW^\pm \rightarrow b\bar{b}W^\pm X$ for backgrounds. Here, the distinction between signal and background is subtle, as the final state tbH^\pm enters as signal for the decay $H^\pm \rightarrow \tau\nu_\tau$ but as background for $\Phi^0 \rightarrow b\bar{b}$ because of the top decay $t \rightarrow bX$. In the signal versus background analysis we treated the rates of tbH^\pm exactly on this footing: when we compute the numbers for the signals separately, tbH^\pm was considered background to $H^\pm\Phi^0 X$, whereas, in the ‘inclusive’ case $H^\pm X$ (i.e., when we summed up the rates of $H^\pm\Phi^0 X$ and $tbH^\pm \rightarrow b\bar{b}H^\pm X$), they contributed to the event rates only. In computing the the signal-to-noise ratios we ignored the case of the H^0 in $H^\pm\Phi^0 X$ (whose rates are never greater than ≈ 0.4 fb).

For the two values $\tan\beta = 1.5$ and 30 and in the range $60 \text{ GeV} \lesssim M_{A^0} \lesssim 140 \text{ GeV}$ the mass of the charged Higgs is always larger than $\approx 100 \text{ GeV}$. Therefore W^\pm - and H^\pm -peaks do not overlap in the spectrum of the invariant mass $M_{\tau\nu_\tau}$ and charged Higgs signal should be clearly recognised, whereas the case $H^\pm\Phi^0 X$ is largely covered by the backgrounds (we found that significancies are always smaller than 1 after one year of running). So, the signature $\tau\nu_\tau b\bar{b}$ definitely gives large chances of charged Higgs detection (for all masses and $\tan\beta$ ’s), whereas this latter is hopeless in the case of neutral Higgses.

D. Signature $\tau\nu_\tau\tau\nu_\tau$.

This channel has signal contributions from double charged Higgs production $H^+H^- X$ and backgrounds from charged vector boson production $W^+W^- X$, as well as from neutral production $Z^0 Z^0 X$ (with one Z^0 decaying to $\tau^+\tau^-$ pairs and the other to neutrinos). Both the processes with H^\pm ’s and W^\pm ’s benefit from a large top-resonant component ($q = b$ in eq. (29)), but only backgrounds rates have significant contributions for $q \neq b$. The case $Z^0 Z^0 X$ has a much smaller cross section. A few words are needed here to discuss the strategy for detecting Higgs signals, as the presence of two neutrinos should prevent from reconstructing invariant mass spectra. For example, one possibility could simply be the one of looking at the total rates in $\tau\nu_\tau\tau\nu_\tau$ events. An excess of $2\tau 2\nu_\tau$ events (i.e., a breaking of the τ vs μ/e universality), with respect to the numbers expected from $W^+W^- X$ plus $Z^0 Z^0 X$ production, could well be the method of establishing the presence of H^\pm signals. In that way, these latter should be clearly disentangled over all the intermediate mass range, for both values of $\tan\beta = 1.5$ and 30, presumably after just one year of running.

E. Signature $jj\tau\nu_\tau$.

To this channel there is a signal contribution coming from $q\bar{q}'H^\pm X$ when $q\bar{q}' \neq t\bar{b}$, whereas backgrounds come from $W^\pm Z^0 X$ (with $Z^0 \rightarrow jj$) and $W^+W^- X$ events (with one $W^\pm \rightarrow jj$). As $M_{H^\pm} - M_{W^\pm} \gtrsim 20 \text{ GeV}$ over the $(M_{A^0}, \tan\beta)$ region here considered, the detection of H^\pm -signal should only be a matter of event rates. For $\tan\beta = 1.5$ numbers are very small, $\lesssim \mathcal{O}(10^{-1})$. In tab. VIb the cross section of the process $ep \rightarrow q\bar{q}'H^\pm$ for $q\bar{q}' \neq t\bar{b}$ is $\approx 23(16)[9]\{7\} < 4 > \text{ fb}$, for $M_{A^0} = 60(80)[100]\{120\} < 140 > \text{ GeV}$ and $\tan\beta = 30$.

Therefore, we expect the signature $jj\tau\nu_\tau$ to give further chances to detect \mathcal{MSSM} charged Higgses at large $\tan\beta$, generally over all the intermediate mass range of the A^0 .

We are aware that, in order to conclude our analysis in a realistic manner, some additional steps would be necessary now. For example, the gauge bosons W^\pm and Z^0 that we have kinematically constrained so far to be on-shell should be allowed to decay. The same should be done for the \mathcal{MSSM} Higgs bosons H^0, h^0, A^0 and H^\pm . In addition, the final state partons should be evolved into hadrons and reconstructed from the detector acceptances. Therefore, on the one hand, a clustering scheme of the jets should be adopted while, on the other hand, information about the detector design (azimuthal coverage, cell structure, etc ...) and performances (in particle identification, in microvertex efficiency, etc ...) should be properly included into the phenomenological simulation.

Nevertheless, we have not done all of this. We have decided not to do that for two substantial reasons, related to the subject of the kinematical acceptances. First, doing this would have required a not negligible computing effort, because of the large numbers of different processes with different kinematics here involved (both among signals and backgrounds). Second, such effort could have risked being finalised in a wrong direction, in the sense that our choice of kinematical cuts could have well been different from the one which will be imposed by the real detectors. At present, in fact, the acceptances of the detectors of the LEP \otimes LHC are difficult to predict, as the most recent and complete studies on the argument only deal with simulations done for the LHC (see the ATLAS [59] and CMS [60] Technical Proposals). That is, we wonder if the detectors designed for a pp machine will be the same and/or will work in the same configuration even when they will be set up around a different kind of machine, an ep collider.

However, in order not to leave this issue completely un-addressed, we borrow some numbers from ref. [48], where a complete analysis was attempted. There, the following cuts

- transverse momentum p_T^i of at least 20 GeV;
- pseudorapidity $|\eta_i|$ less than 4.5;
- separation $\Delta R_{ij} = \sqrt{\Delta\eta_{ij} + \Delta\varphi_{ij}} > 1$;

were assumed [37], for all the i -th and j -th b 's and jets in the the signature $b\bar{b}jj$ of the \mathcal{SM} , which would correspond here to the one obtained in the case of process (2) for $\Phi^0 = h^0$ and $\tan\beta = 1.5$ (i.e., with M_{h^0} between ≈ 60 and ≈ 80 GeV). We concentrate only on this case since this is the one where the effects of the (continuum) backgrounds are effective but nevertheless still do not prevent detecting h^0 -signals.

After applying the above kinematical requirements, reduction factors of $\approx 16 - 7$ for the signal $W^\pm\phi$, with $M_\phi = 60 - 140$ GeV¹⁷, and of $\approx 14/11$ for the $t\bar{b}X/t\bar{t}X$ backgrounds were found. As the only differences between the \mathcal{SM} case of ref. [48] and the \mathcal{MSSM} one studied here (when $M_{h^0} = M_\phi$) consists in the presence of some angular factors in

¹⁷Here ϕ represents the \mathcal{SM} Higgs boson and M_ϕ its mass.

the *SUSY* vertices of reaction (2) (see tabs. A.I–A.IV in the Appendix) and different (but small) top width effects in the backgrounds (the substitution $\Gamma_t^{SM} \rightarrow \Gamma_t^{MSSM}$), the numbers we obtained there can be safely used for the present case too. Therefore, even though the kinematical acceptances act in the direction of favouring the backgrounds, by reducing the signal-versus-noise ratio and largely spoiling the effectiveness of the $M_{bW \rightarrow bj\bar{j}}$ cut (see ref. [48]), in our opinion such effects should not have a decisive impact on the feasibility of the h^0 detection in $jjb\bar{b}$ events. We think the same holds also for the other signatures, especially because their background events have discrete spectra in the invariant masses of the Higgs decay products, and the requirements $M_{H^\pm} \approx M_{\tau\nu\tau}$ and/or $M_{\Phi^0} \approx M_{b\bar{b}}$ should be generally sufficient to give large significancies, such that an eventual reduction due to kinematical cuts shouldn't modify the detection strategies we indicated.

Although our analysis remains partially incomplete, we believe that the purpose of our study has been reached. This was in fact to give some hints in the direction of analysing the impact of using back-scattered photons in γp -initiated collisions at the proposed CERN LEP \otimes LHC collider, trying to establish whether such a machine could give additional informations in the study of the Higgs sector of the *MSSM*, once the potential of the two colliders LEP and LHC (separately operating) was already fully exploited. This is especially relevant if one considers the possibility that a long gap in time between the end of the LEP and LHC era and the beginning of the NLC one could happen in the future of particle physics.

A brief summary of what we have been doing and the answers to the above considerations are left in the next section.

Summary and conclusions

We have studied in this paper some production mechanisms of the Higgs bosons of the *MSSM* (i.e., H^0, h^0, A^0 and H^\pm) and of the possible backgrounds to their signatures at the proposed LEP \otimes LHC ep collider at CERN.

Such a machine can be obtained by crossing an electron/positron beam from LEP with a proton one from the LHC. It should presumably run with a CM energy at the TeV scale and with a luminosity between one and ten inverse picobarns per year. Its discovery/detection potential in the Higgs sector was already analysed for the case where the collider is assumed to operate in the ep mode (i.e., via electron-quark and electron-gluon scatterings). Promising results were found for the case of Higgs bosons with intermediate mass, especially if high b -tagging performances can be achieved in detecting neutral Higgses decaying to $b\bar{b}$ -pairs. We addressed here the same matter, but assuming the accelerator working in a possible γp mode, with the incoming photons produced through Compton back-scattering of laser light against the electron/positron beam. This technique has received a lot of attention in the past few years as a concrete possibility of setting up real $e\gamma$ and $\gamma\gamma$ interactions at e^+e^- linear colliders of the next generation. Such photonic interactions are expected to take place with almost the same characteristics (in energy of the beams and in integrated luminosity) as the e^+e^- ones. We studied the possibility of producing γp interactions at CERN as we expect the design of the LEP \otimes LHC machine not to prevent the application of the laser back-scattering method.

Independently of the fact that *SUSY* Higgs bosons could have already been found either

at LEP or LHC, the CERN “ γp machine” would have a clear importance on its own, since the fundamental interactions would take place here via γ -quark and γ -gluon scatterings, these proceeding via a large number of \mathcal{MSSM} vertices, which can then be tested. Photons, in fact, directly couple at leading order to the \mathcal{MSSM} (charged) Higgs scalars, whereas electrons/positrons don’t (because of the negligible mass of the electron in the Yukawa couplings). Therefore, at the NLC, very few Higgs production mechanisms and a reduced number of fundamental vertices are involved.

Both the high ep energy available at the LEP \otimes LHC and the properties of the back-scattered photons would make the production of Higgs events with high rates possible. Moreover, the absence of strong interactions from the initial state, which take place at hadron colliders (via $q\bar{q}$, gg and qg scatterings), would make the CERN machine the first TeV environment partially free from the huge QCD noise typical of the LHC (and of the Tevatron as well). Finally, both the technology and the expenses needed in converting two machines already existing (such as LEP and LHC) and physically located in the same place (even though maybe not at the same time) has to be considered, compared to building a new one (the NLC): this could make conceivable to expect the CERN ep accelerator to be operating well in advance of any future linear collider.

For obvious reasons of space (in reducing the huge amount of material to a size compatible with a journal publication) and time (in numerically computing cross sections and distributions of both signals and backgrounds), we concentrated only on a limited region of the \mathcal{MSSM} parameter space ($M_{A^0}, \tan\beta$). Because of kinematical constrains imposed by the collider energy and luminosity, we studied Higgs scalars in the intermediate mass interval whereas, as example of two opposite situations, we chose two values at the extremes of the available range of $\tan\beta$ (that is, 1.5 and 30). Our work turns out to be incomplete then. However, as the discussion of the results has been carried on by stressing their dependence on the masses and on the couplings of the \mathcal{MSSM} Higgs scalars, we expect our analysis to be easily translatable to the case in which different values of M_{A^0} and/or $\tan\beta$ are adopted. Some remarks are also in order concerning the treatment of the signals, of the backgrounds and the approach to the kinematical cuts.

On the one hand, we assumed a 100% b -tagging efficiency, thus neglecting considering light quark and gluon jets faking b ’s in the Higgs decays $\Phi^0 \rightarrow b\bar{b}$. This is obviously unrealistic but, by the time of the advent of the LEP \otimes LHC, b -tagging performances should be very high, and not too far from the above ideal case. In addition, signals and discrete backgrounds involving Higgses, Z^0 and W^\pm decaying into $b\bar{b}$ and $\tau\nu_\tau$ (the signatures of neutral and charged Higgs scalars we have studied here, respectively) have been computed keeping the bosons on-shell, and considering the invariant mass of their decay products to fill a region of only 10 GeV around the corresponding peak. Such an approximation should be clearly dropped in the end, in order to predict reliable numbers. However, as we clearly identified as regions of feasible detection of the \mathcal{MSSM} Higgs particles especially the ones well far from the Z^0 - and W^\pm -resonances, we expect the inclusion of the tails of the Breit-Wigner distributions not to substantially modify our conclusions. In fact, most of the cases in which Higgs and gauge boson peaks overlap seem to be already out of the experimental possibilities in the on-shell approximation.

On the other hand, a full analysis (including kinematical cuts, detector efficiencies,

hadronization effects, etc ...) was far beyond our intentions, mainly because a detailed simulation should necessarily rely on the precise knowledge of the characteristics of the LEP⊗LHC detectors, which we cannot have at the moment. In this respect, a possible way to proceed could well have been, for example, the one of taking the details needed for this study from the recent ATLAS [59] and CMS [60] Technical Proposals for the LHC, which are probably the most complete and up to date source of useful information. Nevertheless, we expect that by the time the CERN ep collider will be operating, both the improvement in the techniques and the necessity to adjust the detectors in view of their best performances at a different kind of machine (ep instead of pp), could end up indicating event selection criteria different from the ones we could suppose now. What we instead preferred to do here was to take, as example, a similar study we performed in the case of the \mathcal{SM} in a previous paper, in order to show how in general kinematical cuts should have a decisive impact on the signal significancies only where these are very small, thus affecting only restricted regions of the \mathcal{MSSM} parameter space here considered. Leaving practically intact in the rest of the cases the chances of Higgs detections and studies.

Under such premises, we demonstrated the high potential of the LEP⊗LHC. What we obtained is that in some parts of the parameter region we studied all the \mathcal{MSSM} Higgs bosons could be contemporaneously detected (especially if a high luminosity can be achieved). However, where this does not happen, at least two of them are accessible to the experiment and it is never the case that none of the the Higgs scalars can be recognised. For all the neutral bosons (H^0, h^0 and A^0) we considered the $b\bar{b}$ decay channel, whereas for the charged Higgses (H^{\pm} 's) we studied the decay mode $\tau\nu_\tau$. The signatures we assumed are in $b\bar{b}b\bar{b}$, $jjb\bar{b}$, $\tau\nu_\tau b\bar{b}$, $\tau\nu_\tau\tau\nu_\tau$ and $jj\tau\nu_\tau$ events. In detail, the most favourable cases are the following.

For the heavy scalar H^0 good chances of detection happen when $\tan\beta = 30$ in the case of the $4b$ -signature, via the production subprocess $g\gamma \rightarrow b\bar{b}H^0$, if $M_{A^0} \gtrsim 120$ GeV ($M_{H^0} \gtrsim 130$ GeV). The remaining mass range $M_{A^0} \lesssim 120$ GeV ($M_{H^0} \lesssim 130$ GeV) is quite difficult to cover, as the only possible way would be via the signature $jjb\bar{b}$, through the production processes $q\gamma \rightarrow q'W^\pm H^0$ and $q\gamma \rightarrow qZ^0 H^0$ (the first one mostly), which have large production rates but small significancies (large continuum backgrounds). A high luminosity option would be needed in this case (say, tens of inverse femtobarns per year) to clearly extract H^0 -signals. If $\tan\beta = 1.5$ the situation is even less optimistic. Only after a few years of running at the standard luminosity $\mathcal{L} = 3 \text{ fb}^{-1}$ it should be possible to recognize a few $W^\pm H^0$ events, and these would not be probably enough for attempting a statistically significant study. Therefore, we would conclude that for the \mathcal{MSSM} neutral heavy scalar the parameter region at small $\tan\beta$ would remain practically uncovered, whereas the one at large $\tan\beta$'s should be accessible by the experiment if $M_{H^0} \gtrsim 130$ GeV (for a standard \mathcal{L}).

The light neutral Higgs h^0 , even with its reduced mass if compared to M_{H^0} , has definitely much more chances to be detected. The production in events $W^\pm h^0 X$ (giving the signature $jjb\bar{b}$) is quite large if $\tan\beta = 1.5$. As $M_{Z^0} - M_{h^0} \gtrsim 10$ GeV over all the interval $60 \text{ GeV} \lesssim M_{A^0} \lesssim 140 \text{ GeV}$ and the cut in $M_{bW \rightarrow bjj}$ can be successfully exploited in rejecting tbX and $t\bar{t}X$ events, h^0 -signals should be disentangled from the backgrounds up to the maximum value of $M_{h^0} \approx 81$ GeV. A few units of events per year in the above signature would come from $Z^0 h^0 X$ production too. The cases of $H^\pm h^0 X^-$, $h^0 A^0 X^-$ and $q\bar{q}h^0 X^-$ -production do not deserve much attention (very small cross sections). If $\tan\beta = 30$, good candidates

are $W^\pm h^0 X$ events, provided that $M_{h^0} \gtrsim 120$ GeV ($M_{A^0} \gtrsim 120$ GeV). The most probable signature would be again $jj\bar{b}b$. The case $Z^0 h^0 X$ at $\tan\beta = 30$ is completely beyond any experimental possibility. Production events of the type $H^\pm h^0$ and $h^0 A^0 X$ contribute by adding some more chances of h^0 -detection if $\tan\beta = 30$ only in the case $M_{h^0} \approx M_{A^0} \approx 60$ GeV (via the signatures $\tau\nu_\tau\bar{b}b$ and $b\bar{b}b\bar{b}$, respectively). The case where the rewards for h^0 -detection at high $\tan\beta$'s are largest is probably via the subprocess $g\gamma \rightarrow b\bar{b}h^0$, if $M_{h^0} \approx M_{A^0} \lesssim 120$ GeV. The production rates are in fact extremely large and the $4b$ -signature is clean from backgrounds, provided that high b -tagging performances can be achieved and M_{h^0} is far enough from M_{Z^0} . Therefore, for the \mathcal{MSSM} neutral light scalar, we conclude that both the regions $\tan\beta = 1.5$ and 30 are adequately covered, and h^0 -signals are observable.

The pseudoscalar Higgs A^0 is practically uncovered if $\tan\beta = 1.5$ and $M_{A^0} \gtrsim 80$ GeV. In fact, a few chances at small $\tan\beta$'s occur only when $M_{A^0} \approx 60$ GeV, via the signature $\tau\nu_\tau\bar{b}b$ in $H^\pm A^0 X$ events and only after a few years of running. The large $\tan\beta$ region case is instead entirely covered via the $g\gamma \rightarrow b\bar{b}A^0$ production mechanism. Even in the case that the final efficiencies and purities in b -tagging are smaller than the ones expected now, the large production rates should guarantee the detection of the A^0 in the $4b$ -mode. In the case of the \mathcal{MSSM} neutral pseudoscalar Higgs then, only the large $\tan\beta$ region is fully covered, whereas the remaining one is really difficult, as even the most favourable case $M_{A^0} \approx 60$ GeV needs a lot of integrated luminosity.

Finally, the case of the charged Higgses. Both single and double H^\pm -production give account of large production rates, at both $\tan\beta$'s. As $M_{H^\pm} - M_{W^\pm} \gtrsim 10$ GeV, backgrounds should be manageable. Therefore, we expect that in the intermediate mass range of the A^0 (which correspond to the values 100 GeV $\lesssim M_{H^\pm} \lesssim 160$ GeV) charged Higgses should be recognised and detected, both at small and at large values of $\tan\beta$.

In conclusion then, although we recognise that a more complete study (especially involving a coverage of the whole \mathcal{MSSM} parameter space) is needed, together with a more refined signal versus background analysis (once the performances expected from the detectors of the LEP \otimes LHC will become clear), we stress that the possibilities of the proposed CERN ep collider in testing the Higgs sector of the \mathcal{MSSM} are encouraging indeed, with the machine operating in the γp mode. Therefore, such a project should be seriously kept into consideration, especially if LEP and LHC together will not be able to confirm or rule out with certainty the \mathcal{MSSM} .

Acknowledgments

We are grateful to J.B. Tausk for interesting discussions and useful suggestions during the early stages of this work, to T. Stelzer for his helpful advice in using MadGraph and, finally, to W.J. Stirling for reading the manuscript.

Appendix

In this section we give the explicit formulae for the helicity amplitudes of the processes we have studied. Definitions of S , Y and Z functions and of other quantities (p , λ , μ , η , etc...), which enter in the following, can be found in ref. [28], with identical notations.

Here, we introduce the definitions

$$-b_1 = -b_2 = b_3 = 2b_4 = 2b_5 = 2b_6 = 2b_7 = 1 \quad (41)$$

for the coefficients of the incoming/outgoing four-momenta,

$$D_V(p) = \frac{1}{p^2 - M_V^2}, \quad D_q(p) = \frac{1}{p^2 - m_q^2} \quad (42)$$

for the propagators, where $V = W^\pm, H^\pm, Z^0$ or γ and $q = u$ or d ,

$$N_i = [4(p_i \cdot q_i)]^{-1/2}, \quad i = 1, 2 \quad (43)$$

for the gluon ($i = 1$) and the photon ($i = 2$) normalisation factor, where $p_i(q_i)$ is the massless vector four-momentum (any four-vector not proportional to p_i), with $i = 1, 2$ [42]. The symbols r_1 and r_2 represent two light-like four-momenta satisfying the relations

$$r_1^2 = r_2^2 = 0, \quad r_1^\mu + r_2^\mu = p_4^\mu, \quad (44)$$

($d\Omega_{r_1(r_2)}$ indicates the solid angle of $r_{1(2)}$ in the rest frame of p_4) [42], p_6 and p_7 are antispinor four-momenta such that

$$p_6^\mu \equiv p_4^\mu, \quad p_7^\mu \equiv p_5^\mu, \quad (45)$$

and

$$\sum_{\lambda=\pm} u(p_i, \lambda) \bar{u}(p_i, \lambda) = \not{p}_i - m_i, \quad \text{with } i = 6, 7, \quad (46)$$

while

$$\sum_{\lambda=\pm} u(p_i, \lambda) \bar{u}(p_i, \lambda) = \not{p}_i + m_i, \quad \text{with } i = 4, 5. \quad (47)$$

We also define the mass relation

$$\begin{aligned} \Delta_{\Phi, \Phi'}^V &= \frac{M_\Phi^2 - M_{\Phi'}^2}{M_V^2} & \text{if } \Phi \neq \Phi' \ (M_V \neq 0), \\ &= 0 & \text{if } \Phi = \Phi', \end{aligned} \quad (48)$$

the additional coefficients

$$\begin{aligned} c_{\Phi, \Phi'; i}^V &= (1 - \Delta_{\Phi, \Phi'}^V) b_i, & \text{for } i = 4 \text{ and } 6, \\ c_{\Phi, \Phi'; i}^V &= -(1 + \Delta_{\Phi, \Phi'}^V) b_i, & \text{for } i = 5 \text{ and } 7, \end{aligned} \quad (49)$$

where V and Φ, Φ' represent vector and Higgs bosons, respectively, and the spinor functions¹⁸

$$\mathcal{X}_2 = \sum_{\lambda=\pm} \sum_{i=1,3} (-b_i) Y([2]; [i]; 1, 1) Y([i]; (2); 1, 1),$$

¹⁸We adopt the symbol $\{\lambda\}$ to denote a set of helicities of all external particles in a given reaction, $\sum_{\{\lambda\}}$ to indicate the usual sum over all their possible combinations, and the symbol $\sum_{i=j,k,l,\dots}$ to indicate a sum over j, k, l, \dots with index i .

$$\begin{aligned}
\mathcal{X}_4 &= \sum_{\lambda=\pm} \sum_{i=5,7} b_i Y(\{1\}; [i]; 1, 1) Y([i]; \{2\}; 1, 1), \\
\mathcal{X}_{31}^{qV^{(\prime)}} &= \sum_{\lambda=\pm} \sum_{i=4,6(5,7)} b_i Y([3]; [i]; 1, 1) Y([i]; [1]; c_{R_V}^q, c_{L_V}^q), \\
\mathcal{Y}_2^{(\prime)} &= \sum_{\lambda=\pm} \sum_{i=4,6(5,7)} b_i Y([2]; [i]; 1, 1) Y([i]; (2); 1, 1), \\
\mathcal{Y}_4 &= \sum_{\lambda=\pm} Y(\{1\}; p_2, \lambda; 1, 1) Y(p_2, \lambda; \{2\}; 1, 1), \\
\mathcal{F}_{31}^{qV} &= \mu_1 \eta_1 Y([3]; [1]; c_{L_V}^q, c_{R_V}^q) - \mu_3 \eta_3 Y([3]; [1]; c_{R_V}^q, c_{L_V}^q), \\
\mathcal{Y}_{31}^{qV} &= \sum_{\lambda=\pm} Y([3]; p_2, \lambda; 1, 1) Y(p_2, \lambda; [1]; c_{R_V}^q, c_{L_V}^q), \\
\tilde{\mathcal{Y}}_{31}^{qV} &= \mathcal{Y}_{31}^{qV} - \frac{\mathcal{F}_{31}^{qV}}{M_V^2} p_2 \cdot (p_4 + p_5), \\
\mathcal{Z}_{24} &= Z([2]; (2); \{1\}; \{2\}; 1, 1, 1, 1), \\
\mathcal{Z}_{312}^{qV} &= Z([3]; [1]; [2]; (2); c_{R_V}^q, c_{L_V}^q; 1, 1), \\
\tilde{\mathcal{Z}}_{312}^{qV} &= \mathcal{Z}_{312}^{qV} - \frac{\mathcal{F}_{31}^{qV}}{M_V^2} (\mathcal{Y}_2 + \mathcal{Y}'_2), \\
\mathcal{Z}_{314}^{qV} &= Z([3]; [1]; \{1\}; \{2\}; c_{R_V}^q, c_{L_V}^q; 1, 1), \\
\tilde{\mathcal{Z}}_{314}^{qV} &= \mathcal{Z}_{314}^{qV} - \frac{\mathcal{F}_{31}^{qV}}{M_V^2} (\mathcal{X}_4 - \mathcal{Y}_4), \tag{50}
\end{aligned}$$

where V represents a gauge boson W^\pm , Z^0 or γ , $q = u$ or d (u - and d -type quarks of arbitrary masses m_u and m_d , respectively), and with the short-hand notations $[x] = p_x$, λ_x ($x = 1, \dots, 4$), $(x) = q_x$, λ_x ($x = 1, 2$) and $\{x\} = r_x$, $-$ ($x = 1, 2$).

In the following we adopt $[i] = p_i$, λ and $[j] = p_j$, λ' , whereas the couplings c_R , c_L and \mathcal{H} can be easily deduced from tabs. A.I–A.IV. Also, we sometimes make use of the equalities

$$\mathcal{Y}_2 + \mathcal{Y}'_2 = \mathcal{X}_2, \quad \mathcal{X}_{31}^{qV} + \mathcal{X}_{31}^{qV'} = \mathcal{Y}_{31}^{qV} + \mathcal{F}_{31}^{qV}. \tag{51}$$

1. Process $d\gamma \rightarrow uW^-\Phi^0$.

In order to obtain from fig. 1 the Feynman graphs of the process

$$d(p_1, \lambda_1) + \gamma(p_2, \lambda_2) \longrightarrow u(p_3, \lambda_3) + W^-(p_4) + \Phi^0(p_5), \tag{52}$$

where $\Phi^0 = H^0, h^0$ or A^0 , one has to make the following assignments:

$$q = d, \quad q' = u, \quad V^{(*)} = W^{\pm(*)}, \quad S^* = H^{\pm*}. \tag{53}$$

The corresponding matrix element, summed over final spins and averaged over initial ones, is given by

$$|\overline{M}| = \frac{e^6}{4} N_2^2 \frac{3}{8\pi M_{W^\pm}^2} \sum_{\{\lambda\}} \int d\Omega_{r_1(r_2)} \sum_{l,m=1}^{17} T_l^{\{\lambda\}} T_m^{\{\lambda\}*}, \quad (54)$$

where

$$\begin{aligned} iT_1^{\{\lambda\}} &= D_u(p_3 + p_5) D_d(p_1 + p_2) M_1^{\{\lambda\}} \mathcal{H}_1, & iT_2^{\{\lambda\}} &= D_d(p_3 + p_4) D_d(p_1 + p_2) M_2^{\{\lambda\}} \mathcal{H}_2, \\ iT_3^{\{\lambda\}} &= D_d(p_3 + p_4) D_d(p_1 - p_5) M_3^{\{\lambda\}} \mathcal{H}_3, & iT_4^{\{\lambda\}} &= D_u(p_3 + p_5) D_u(p_1 - p_4) M_4^{\{\lambda\}} \mathcal{H}_4, \\ iT_5^{\{\lambda\}} &= D_u(p_3 - p_2) D_u(p_1 - p_4) M_5^{\{\lambda\}} \mathcal{H}_5, & iT_6^{\{\lambda\}} &= D_u(p_3 - p_2) D_d(p_1 - p_5) M_6^{\{\lambda\}} \mathcal{H}_6, \\ iT_7^{\{\lambda\}} &= D_{W^\pm}(p_4 + p_5) D_d(p_1 + p_2) M_7^{\{\lambda\}} \mathcal{H}_7, & iT_8^{\{\lambda\}} &= D_{W^\pm}(p_4 + p_5) D_u(p_3 - p_2) M_8^{\{\lambda\}} \mathcal{H}_8, \\ iT_9^{\{\lambda\}} &= D_{H^\pm}(p_4 + p_5) D_d(p_1 + p_2) M_9^{\{\lambda\}} \mathcal{H}_9, & iT_{10}^{\{\lambda\}} &= D_{H^\pm}(p_4 + p_5) D_u(p_3 - p_2) M_{10}^{\{\lambda\}} \mathcal{H}_{10}, \\ iT_{11}^{\{\lambda\}} &= D_{W^\pm}(p_2 - p_4) D_u(p_3 + p_5) M_{11}^{\{\lambda\}} \mathcal{H}_{11}, & iT_{12}^{\{\lambda\}} &= D_{W^\pm}(p_2 - p_4) D_d(p_1 - p_5) M_{12}^{\{\lambda\}} \mathcal{H}_{12}, \\ iT_{13}^{\{\lambda\}} &= D_{W^\pm}(p_1 - p_3) D_{W^\pm}(p_4 + p_5) M_{13}^{\{\lambda\}} \mathcal{H}_{13}, & iT_{14}^{\{\lambda\}} &= D_{W^\pm}(p_1 - p_3) D_{W^\pm}(p_2 - p_4) M_{14}^{\{\lambda\}} \mathcal{H}_{14}, \\ iT_{15}^{\{\lambda\}} &= D_{H^\pm}(p_1 - p_3) D_{H^\pm}(p_4 + p_5) M_{15}^{\{\lambda\}} \mathcal{H}_{15}, & iT_{16}^{\{\lambda\}} &= D_{H^\pm}(p_1 - p_3) D_{W^\pm}(p_2 - p_4) M_{16}^{\{\lambda\}} \mathcal{H}_{16}, \\ & & iT_{17}^{\{\lambda\}} &= D_{H^\pm}(p_1 - p_3) M_{17}^{\{\lambda\}} \mathcal{H}_{17}. \end{aligned} \quad (55)$$

We have

$$\begin{aligned} M_1^{\{\lambda\}} &= \sum_{\lambda=\pm} \sum_{\lambda'=\pm} \sum_{i=3,5,7} \sum_{j=1,2} (-b_i b_j) Y([3]; [i]; c_{R_{\Phi_0}}^u, c_{L_{\Phi_0}}^u) \\ &\quad \times Z([i]; [j]; \{1\}; \{2\}; c_{R_{W^\pm}}, c_{L_{W^\pm}}; 1, 1) Z([j]; [1]; [2]; (2); c_{R_\gamma}^d, c_{L_\gamma}^d; 1, 1), \\ M_2^{\{\lambda\}} &= \sum_{\lambda=\pm} \sum_{\lambda'=\pm} \sum_{i=3,4,6} \sum_{j=1,2} (-b_i b_j) Z([3]; [i]; \{1\}; \{2\}; c_{R_{W^\pm}}, c_{L_{W^\pm}}; 1, 1) \\ &\quad \times Y([i]; [j]; c_{R_{\Phi_0}}^d, c_{L_{\Phi_0}}^d) Z([j]; [1]; [2]; (2); c_{R_\gamma}^d, c_{L_\gamma}^d; 1, 1), \\ M_3^{\{\lambda\}} &= \sum_{\lambda=\pm} \sum_{\lambda'=\pm} \sum_{i=3,4,6} \sum_{j=1,5} (-b_i b_j) Z([3]; [i]; \{1\}; \{2\}; c_{R_{W^\pm}}, c_{L_{W^\pm}}; 1, 1) \\ &\quad \times Z([i]; [j]; [2]; (2); c_{R_\gamma}^d, c_{L_\gamma}^d; 1, 1) Y([j]; [1]; c_{R_{\Phi_0}}^d, c_{L_{\Phi_0}}^d), \\ M_4^{\{\lambda\}} &= \sum_{\lambda=\pm} \sum_{\lambda'=\pm} \sum_{i=3,5,7} \sum_{j=1,4,6} (-b_i b_j) Y([3]; [i]; c_{R_{\Phi_0}}^u, c_{L_{\Phi_0}}^u) \\ &\quad \times Z([i]; [j]; [2]; (2); c_{R_\gamma}^u, c_{L_\gamma}^u; 1, 1) Z([j]; [1]; \{1\}; \{2\}; c_{R_{W^\pm}}, c_{L_{W^\pm}}; 1, 1), \\ M_5^{\{\lambda\}} &= \sum_{\lambda=\pm} \sum_{\lambda'=\pm} \sum_{i=3,2} \sum_{j=1,4,6} (-b_i b_j) Z([3]; [i]; [2]; (2); c_{R_\gamma}^u, c_{L_\gamma}^u; 1, 1) \\ &\quad \times Y([i]; [j]; c_{R_{\Phi_0}}^u, c_{L_{\Phi_0}}^u) Z([j]; [1]; \{1\}; \{2\}; c_{R_{W^\pm}}, c_{L_{W^\pm}}; 1, 1), \\ M_6^{\{\lambda\}} &= \sum_{\lambda=\pm} \sum_{\lambda'=\pm} \sum_{i=3,2} \sum_{j=1,5,7} (-b_i b_j) Z([3]; [i]; [2]; (2); c_{R_\gamma}^u, c_{L_\gamma}^u; 1, 1) \\ &\quad \times Z([i]; [j]; \{1\}; \{2\}; c_{R_{W^\pm}}, c_{L_{W^\pm}}; 1, 1) Y([j]; [1]; c_{R_{\Phi_0}}^d, c_{L_{\Phi_0}}^d), \end{aligned}$$

$$\begin{aligned}
M_7^{\{\lambda\}} &= \sum_{\lambda=\pm} \sum_{i=1,2} (-b_i) Z([i]; [1]; [2]; (2); c_{R_\gamma}^d, c_{L_\gamma}^d; 1, 1) \\
&\quad \times \{Z([3]; [i]; \{1\}; \{2\}; c_{R_{W^\pm}}, c_{L_{W^\pm}}; 1, 1) \\
&\quad - \frac{\mathcal{X}_4}{M_{W^\pm}^2} [\sum_{\lambda'=\pm} \sum_{j=1,2,3} (-b_j) Y([3]; [j]; 1, 1) Y([j]; [i]; c_{R_{W^\pm}}, c_{L_{W^\pm}})]\}, \\
M_8^{\{\lambda\}} &= \sum_{\lambda=\pm} \sum_{i=2,3} (b_i) Z([3]; [i]; [2]; (2); c_{R_\gamma}^u, c_{L_\gamma}^u; 1, 1) \\
&\quad \times \{Z([i]; [1]; \{1\}; \{2\}; c_{R_{W^\pm}}, c_{L_{W^\pm}}; 1, 1) \\
&\quad - \frac{\mathcal{X}_4}{M_{W^\pm}^2} [\sum_{\lambda'=\pm} \sum_{j=1,2,3} (-b_j) Y([i]; [j]; 1, 1) Y([j]; [1]; c_{R_{W^\pm}}, c_{L_{W^\pm}})]\}, \\
M_9^{\{\lambda\}} &= \sum_{\lambda=\pm} \sum_{i=1,2} (-b_i) (-2\mathcal{X}_4) Y([3]; [i]; c_{R_{H^\pm}}, c_{L_{H^\pm}}) Z([i]; [1]; [2]; (2); c_{R_\gamma}^d, c_{L_\gamma}^d; 1, 1), \\
M_{10}^{\{\lambda\}} &= \sum_{\lambda=\pm} \sum_{i=2,3} (b_i) (-2\mathcal{X}_4) Z([3]; [i]; [2]; (2); c_{R_\gamma}^u, c_{L_\gamma}^u; 1, 1) Y([i]; [1]; c_{R_{H^\pm}}, c_{L_{H^\pm}}), \\
M_{11}^{\{\lambda\}} &= \sum_{\lambda=\pm} \sum_{i=3,5,7} (2b_i) Y([3]; [i]; c_{R_{\Phi^0}}^u, c_{L_{\Phi^0}}^u) \\
&\quad \times [\mathcal{Z}_{24} \sum_{\lambda'=\pm} Y([i]; p_2, \lambda'; 1, 1) Y(p_2, \lambda'; [1]; c_{R_{W^\pm}}, c_{L_{W^\pm}}) \\
&\quad - \mathcal{Y}_2 Z(\{1\}; \{2\}; [i]; [1]; 1, 1; c_{R_{W^\pm}}, c_{L_{W^\pm}}) - \mathcal{Y}_4 Z([2]; (2); [i]; [1]; 1, 1; c_{R_{W^\pm}}, c_{L_{W^\pm}})], \\
M_{12}^{\{\lambda\}} &= \sum_{\lambda=\pm} \sum_{i=1,5,7} (-2b_i) Y([i]; [1]; c_{R_{\Phi^0}}^d, c_{L_{\Phi^0}}^d) \\
&\quad \times [\mathcal{Z}_{24} \sum_{\lambda'=\pm} Y([3]; p_2, \lambda'; 1, 1) Y(p_2, \lambda'; [i]; c_{R_{W^\pm}}, c_{L_{W^\pm}}) \\
&\quad - \mathcal{Y}_2 Z(\{1\}; \{2\}; [3]; [i]; 1, 1; c_{R_{W^\pm}}, c_{L_{W^\pm}}) - \mathcal{Y}_4 Z([2]; (2); [3]; [i]; 1, 1; c_{R_{W^\pm}}, c_{L_{W^\pm}})], \\
M_{13}^{\{\lambda\}} &= \mathcal{Z}_{24} (\mathcal{F}_{31}^{W^\pm} + 2\mathcal{Y}'_{31}^{W^\pm}) - 2\mathcal{X}_2 \tilde{\mathcal{Z}}_{314}^{W^\pm} - (2\mathcal{Y}_4 - \mathcal{X}_4) \tilde{\mathcal{Z}}_{312}^{W^\pm} \\
&\quad - \frac{1}{M_{W^\pm}^2} [\mathcal{X}_2 \mathcal{X}_4 (\mathcal{Y}_{31}^{W^\pm} - \mathcal{X}_{31}^{W^\pm} - \mathcal{X}_{31}^{W^\pm'}) + (p_1 - p_3)^2 (\mathcal{Z}_{24} \mathcal{F}_{31}^{W^\pm} + \tilde{\mathcal{Z}}_{312}^{W^\pm} \mathcal{X}_4) + 2p_2 \cdot (p_1 - p_3) \mathcal{Z}_{24} \mathcal{F}_{31}^{W^\pm}] \\
&\quad - \frac{1}{M_{W^\pm}^4} \{[(p_1 - p_3)^2 + p_2 \cdot (p_1 - p_3)] \mathcal{X}_4 (\mathcal{Y}_2 - \mathcal{Y}'_2) \mathcal{F}_{31}^{W^\pm}\}, \\
M_{14}^{\{\lambda\}} &= 2(\tilde{\mathcal{Y}}_{31}^{W^\pm} \mathcal{Z}_{24} - \mathcal{Y}_2 \tilde{\mathcal{Z}}_{314}^{W^\pm} - \mathcal{Y}_4 \tilde{\mathcal{Z}}_{312}^{W^\pm}), \\
M_{15}^{\{\lambda\}} &= 4Y([3]; [1]; c_{R_{H^\pm}}, c_{L_{H^\pm}}) \mathcal{X}_4 (\mathcal{Y}_2 + \mathcal{Y}'_2), \\
M_{16}^{\{\lambda\}} &= -2Y([3]; [1]; c_{R_{H^\pm}}, c_{L_{H^\pm}}) [\mathcal{Z}_{24} p_2 \cdot (p_4 + 2p_5) - 2\mathcal{Y}'_2 \mathcal{Y}_4 - 2\mathcal{Y}_2 \mathcal{X}_4], \\
M_{17}^{\{\lambda\}} &= Y([3]; [1]; c_{R_{H^\pm}}, c_{L_{H^\pm}}) \mathcal{Z}_{24}. \tag{56}
\end{aligned}$$

2. Process $d\gamma \rightarrow dZ^0\Phi^0$.

The Feynman graphs of the process

$$d(p_1, \lambda_1) + \gamma(p_2, \lambda_2) \longrightarrow d(p_3, \lambda_3) + Z^0(p_4) + \Phi^0(p_5), \quad (57)$$

where $\Phi^0 = H^0, h^0$ or A^0 , can be obtained from fig. 1 by setting

$$\begin{aligned} q = q' = d, \quad V^{(*)} &= Z^{0(*)}, \\ M_i^{\{\lambda\}} &= 0, \quad i = 11, \dots, 17, \\ (S^*, \Phi^0) &= (A^{0*}, H^0), \\ &= (A^{0*}, h^0), \\ &= (H^{0*} + h^{0*}, A^0). \end{aligned} \quad (58)$$

The formulae for the amplitude squared corresponding to $\Phi^0 = H^0$ and h^0 are practically the same as in the previous section, with the relabeling:

$$u \rightarrow d, \quad W^\pm \rightarrow Z^0, \quad H^\pm \rightarrow A^0, \quad (59)$$

in eqs. (54)–(56). For the case $\Phi^0 = A^0$, the same relabeling still hold in eq. (54), whereas in eqs.(55)–(56) only for $i = 1, \dots, 8$. For diagrams 9 and 10, one has to introduce in eqs. (55)

$$\begin{aligned} iT_9^{\{\lambda\}} &= D_d(p_1 + p_2)(D_{H^0}(p_4 + p_5)M_{9,H^0}^{\{\lambda\}}\mathcal{H}_{9,H^0} + D_{h^0}(p_4 + p_5)M_{9,h^0}^{\{\lambda\}}\mathcal{H}_{9,H^0}), \\ iT_{10}^{\{\lambda\}} &= D_d(p_3 - p_2)(D_{H^0}(p_4 + p_5)M_{10,H^0}^{\{\lambda\}}\mathcal{H}_{10,H^0} + D_{h^0}(p_4 + p_5)M_{10,h^0}^{\{\lambda\}}\mathcal{H}_{10,h^0}), \end{aligned} \quad (60)$$

with $M_{i,S}^{\{\lambda\}}$, for $i = 9, 10$ and $S = H^0, h^0$, as given in eqs. (56) with the exchanges (59), where $A^0 \rightarrow H^0, h^0$.

3. Process $d\gamma \rightarrow uH^-\Phi^0$.

The Feynman diagrams of the process

$$d(p_1, \lambda_1) + \gamma(p_2, \lambda_2) \longrightarrow u(p_3, \lambda_3) + H^-(p_4) + \Phi^0(p_5), \quad (61)$$

where $\Phi^0 = H^0, h^0$ or A^0 , are depicted in fig. 2, with the assignments:

$$q = d, \quad q' = u, \quad S = H^-, \quad (\Phi, \Phi') = (H^-, \Phi^0), \quad V^* = W^{\pm*}, \quad S^*(S'^*) = H^{\pm*}(H^{\mp*}). \quad (62)$$

The amplitude squared, summed over final spins and averaged over initial ones, is given by

$$|\overline{M}| = \frac{e^6}{4} N_2^2 \sum_{\{\lambda\}} \sum_{l,m=1}^{17} T_l^{\{\lambda\}} T_m^{\{\lambda\}*}, \quad (63)$$

where the $T_i^{\{\lambda\}}$'s, for $i = 1, \dots, 10$, are the same as in eqs. (55) except for a difference in sign, whereas

$$-iT_{11}^{\{\lambda\}} = D_{H^\pm}(p_2 - p_4)D_u(p_3 + p_5)M_{11}^{\{\lambda\}}\mathcal{H}_{11}, \quad -iT_{12}^{\{\lambda\}} = D_{H^\pm}(p_2 - p_4)D_d(p_1 - p_5)M_{12}^{\{\lambda\}}\mathcal{H}_{12},$$

$$\begin{aligned}
-iT_{13}^{\{\lambda\}} &= D_{H^\pm}(p_1-p_3)D_{H^\pm}(p_4+p_5)M_{13}^{\{\lambda\}}\mathcal{H}_{13}, & -iT_{14}^{\{\lambda\}} &= D_{H^\pm}(p_1-p_3)D_{H^\pm}(p_2-p_4)M_{14}^{\{\lambda\}}\mathcal{H}_{14}, \\
-iT_{15}^{\{\lambda\}} &= D_{W^\pm}(p_1-p_3)D_{W^\pm}(p_4+p_5)M_{15}^{\{\lambda\}}\mathcal{H}_{15}, & -iT_{16}^{\{\lambda\}} &= D_{W^\pm}(p_1-p_3)D_{H^\pm}(p_2-p_4)M_{16}^{\{\lambda\}}\mathcal{H}_{16}, \\
& & -iT_{17}^{\{\lambda\}} &= D_{W^\pm}(p_1-p_3)M_{17}^{\{\lambda\}}\mathcal{H}_{17}.
\end{aligned} \tag{64}$$

The spinor amplitudes are

$$\begin{aligned}
M_1^{\{\lambda\}} &= \sum_{\lambda=\pm} \sum_{\lambda'=\pm} \sum_{i=3,5,7} \sum_{j=1,2} (-b_i b_j) Y([3]; [i]; c_{R_{\Phi^0}}^u, c_{L_{\Phi^0}}^u) \\
&\quad \times Y([i]; [j]; c_{R_{H^\pm}}, c_{L_{H^\pm}}) Z([j]; [1]; [2]; (2); c_{R_\gamma}^d, c_{L_\gamma}^d; 1, 1), \\
M_2^{\{\lambda\}} &= \sum_{\lambda=\pm} \sum_{\lambda'=\pm} \sum_{i=3,4,6} \sum_{j=1,2} (-b_i b_j) Y([3]; [i]; c_{R_{H^\pm}}, c_{L_{H^\pm}}) \\
&\quad \times Y([i]; [j]; c_{R_{\Phi^0}}^d, c_{L_{\Phi^0}}^d) Z([j]; [1]; [2]; (2); c_{R_\gamma}^d, c_{L_\gamma}^d; 1, 1), \\
M_3^{\{\lambda\}} &= \sum_{\lambda=\pm} \sum_{\lambda'=\pm} \sum_{i=3,4,6} \sum_{j=1,5} (-b_i b_j) Y([3]; [i]; c_{R_{H^\pm}}, c_{L_{H^\pm}}) \\
&\quad \times Z([i]; [j]; [2]; (2); c_{R_\gamma}^d, c_{L_\gamma}^d; 1, 1) Y([j]; [1]; c_{R_{\Phi^0}}^d, c_{L_{\Phi^0}}^d), \\
M_4^{\{\lambda\}} &= \sum_{\lambda=\pm} \sum_{\lambda'=\pm} \sum_{i=3,5,7} \sum_{j=1,4,6} (-b_i b_j) Y([3]; [i]; c_{R_{\Phi^0}}^u, c_{L_{\Phi^0}}^u) \\
&\quad \times Z([i]; [j]; [2]; (2); c_{R_\gamma}^u, c_{L_\gamma}^u; 1, 1) Y([j]; [1]; c_{R_{H^\pm}}, c_{L_{H^\pm}}), \\
M_5^{\{\lambda\}} &= \sum_{\lambda=\pm} \sum_{\lambda'=\pm} \sum_{i=3,2} \sum_{j=1,4,6} (-b_i b_j) Z([3]; [i]; [2]; (2); c_{R_\gamma}^u, c_{L_\gamma}^u; 1, 1) \\
&\quad \times Y([i]; [j]; c_{R_{\Phi^0}}^u, c_{L_{\Phi^0}}^u) Y([j]; [1]; c_{R_{H^\pm}}, c_{L_{H^\pm}}; 1, 1), \\
M_6^{\{\lambda\}} &= \sum_{\lambda=\pm} \sum_{\lambda'=\pm} \sum_{i=3,2} \sum_{j=1,5,7} (-b_i b_j) Z([3]; [i]; [2]; (2); c_{R_\gamma}^u, c_{L_\gamma}^u; 1, 1) \\
&\quad \times Y([i]; [j]; c_{R_{H^\pm}}, c_{L_{H^\pm}}) Y([j]; [1]; c_{R_{\Phi^0}}^d, c_{L_{\Phi^0}}^d), \\
M_7^{\{\lambda\}} &= \sum_{\lambda=\pm} \sum_{\lambda'=\pm} \sum_{i=4,5,6,7} \sum_{j=1,2} (-c_{H^-, \Phi^0; i}^{W^\pm} b_j) Y([3]; [i]; 1, 1) Y([i]; [j]; c_{R_{W^\pm}}, c_{L_{W^\pm}}) \\
&\quad \times Z([j]; [1]; [2]; (2); c_{R_\gamma}^d, c_{L_\gamma}^d; 1, 1), \\
M_8^{\{\lambda\}} &= \sum_{\lambda=\pm} \sum_{\lambda'=\pm} \sum_{i=2,3} \sum_{j=4,5,6,7} (b_i c_{H^-, \Phi^0; j}^{W^\pm}) Z([3]; [i]; [2]; (2); c_{R_\gamma}^u, c_{L_\gamma}^u; 1, 1) \\
&\quad \times Y([i]; [j]; 1, 1) Y([j]; [1]; c_{R_{W^\pm}}, c_{L_{W^\pm}}), \\
M_9^{\{\lambda\}} &= \sum_{\lambda=\pm} \sum_{i=1,2} (-b_i) Y([3]; [i]; c_{R_{H^\pm}}, c_{L_{H^\pm}}) Z([i]; [1]; [2]; (2); c_{R_\gamma}^d, c_{L_\gamma}^d; 1, 1), \\
M_{10}^{\{\lambda\}} &= \sum_{\lambda=\pm} \sum_{i=2,3} (b_i) Z([3]; [i]; [2]; (2); c_{R_\gamma}^u, c_{L_\gamma}^u; 1, 1) Y([i]; [1]; c_{R_{H^\pm}}, c_{L_{H^\pm}}), \\
M_{11}^{\{\lambda\}} &= \sum_{\lambda=\pm} \sum_{i=3,5,7} (b_i) (-2\mathcal{Y}_2) Y([3]; [i]; c_{R_{\Phi^0}}^u, c_{L_{\Phi^0}}^u) Y([i]; [1]; c_{R_{H^\pm}}, c_{L_{H^\pm}}),
\end{aligned}$$

$$\begin{aligned}
M_{12}^{\{\lambda\}} &= \sum_{\lambda=\pm} \sum_{i=1,5,7} (-b_i)(-2\mathcal{Y}_2)Y([3]; [i]; c_{R_{H^\pm}}, c_{L_{H^\pm}})Y([i]; [1]; c_{R_{\Phi^0}}, c_{L_{\Phi^0}}^d), \\
M_{13}^{\{\lambda\}} &= (-2\mathcal{X}_2)[2Y([3]; [1]; c_{R_{H^\pm}}, c_{L_{H^\pm}})], \\
M_{14}^{\{\lambda\}} &= (-2\mathcal{Y}_2)[2Y([3]; [1]; c_{R_{H^\pm}}, c_{L_{H^\pm}})], \\
M_{15}^{\{\lambda\}} &= [c_{H^-\Phi^0;4}^{W^\pm}\mathcal{Y}_2 + c_{H^-\Phi^0;5}^{W^\pm}\mathcal{Y}'_2][2\tilde{\mathcal{Y}}_{31}^{W^\pm} + (1 - \frac{(p_1 - p_3)^2}{M_{W^\pm}^2})\mathcal{F}_{31}^{W^\pm}] \\
&\quad - 2\mathcal{X}_2\{[\mathcal{X}_{31}^{W^\pm} - \frac{\mathcal{F}_{31}^{W^\pm}}{M_{W^\pm}^2}p_4 \cdot (p_1 - p_3)]c_{H^-\Phi^0;4}^{W^\pm} + [\mathcal{X}_{31}^{W^{\pm'}} - \frac{\mathcal{F}_{31}^{W^\pm}}{M_{W^\pm}^2}p_5 \cdot (p_1 - p_3)]c_{H^-\Phi^0;5}^{W^\pm}\} \\
&\quad + (p_4 + p_5 - 2p_2) \cdot (c_{H^-\Phi^0;4}^{W^\pm}p_4 + c_{H^-\Phi^0;5}^{W^\pm}p_5)\tilde{\mathcal{Z}}_{312}^{W^\pm}, \\
M_{16}^{\{\lambda\}} &= (-2\mathcal{Y}_2)[\mathcal{F}_{31}^{W^\pm} - 2\mathcal{X}_{31}^{W^{\pm'}} - \frac{(p_1 - p_3) \cdot (p_1 - p_3 - 2p_5)}{M_{W^\pm}^2}\mathcal{F}_{31}^{W^\pm}], \\
M_{17}^{\{\lambda\}} &= \tilde{\mathcal{Z}}_{312}^{W^\pm} - \frac{\mathcal{F}_{31}^{W^\pm}\mathcal{X}_2}{M_{W^\pm}^2}. \tag{65}
\end{aligned}$$

4. Process $d\gamma \rightarrow d\Phi^0\Phi^{0'}$.

The Feynman diagrams which describe the reaction

$$d(p_1, \lambda_1) + \gamma(p_2, \lambda_2) \longrightarrow d(p_3, \lambda_3) + \Phi^0(p_4) + \Phi^{0'}(p_5), \tag{66}$$

where $\Phi^0, \Phi^{0'} = H^0, h^0$ or A^0 , are reported in fig. 2, where

$$q = q' = d, \quad (\Phi, \Phi') = (\Phi^0, \Phi^{0'}), \quad V^* = Z^{0*},$$

with

$$M_i^{\{\lambda\}} = 0, \quad i = 11, \dots, 17,$$

and the combinations

$$\begin{aligned}
(S^*, \Phi^0, \Phi^{0'}) &= (H^{0*} + h^{0*}, H^0, H^0), \\
&= (H^{0*} + h^{0*}, H^0, h^0), \\
&= (A^{0*}, H^0, A^0), \\
&= (H^{0*} + h^{0*}, h^0, h^0), \\
&= (A^{0*}, h^0, A^0), \\
&= (H^{0*} + h^{0*}, A^0, A^0). \tag{67}
\end{aligned}$$

The amplitude squared is given by a formula identical to eq. (63). The expressions for the spinor functions and the propagators are the same as in eqs. (65) for the combinations (A^{0*}, H^0, A^0) and (A^{0*}, h^0, A^0) , after the exchanges:

$$u \rightarrow d, \quad W^\pm \rightarrow Z^0, \quad H^\pm \rightarrow A^0. \tag{68}$$

For the cases in eq. (67) with double-flavoured Higgs propagators, eqs. (64)–(65) hold for the indices $i = 1, \dots, 8$, while for diagrams 9 and 10, one has to introduce the same equations as in (60) and the same $M_{i,S}^{\{\lambda\}}$'s, for $i = 9, 10$ and $S = H^0, h^0$, as given in eqs. (65) with the exchanges (68), where $A^0 \rightarrow H^0, h^0$.

5. Process $d\gamma \rightarrow dH^-H^+$.

The Feynman diagrams for

$$d(p_1, \lambda_1) + \gamma(p_2, \lambda_2) \longrightarrow d(p_3, \lambda_3) + H^-(p_4) + H^+(p_5), \quad (69)$$

are again displayed in fig. 2, where now

$$q = q' = d, \quad (\Phi, \Phi') = (H^-, H^+), \quad V^* = \gamma^* + Z^{0*}, \quad S^* = H^0 + h^0, \quad S^{*'} = H^{\pm*},$$

$$M_i^{\{\lambda\}} = 0, \quad \text{for } i = 2, 3, 6, \quad (70)$$

and where, moreover, one has to exchange $\Phi \leftrightarrow \Phi'$ in diagram 12 and replace diagrams 13 and 15, by 14 and 16, respectively, but with $\Phi \leftrightarrow \Phi'$. The matrix element is given by the formula (63), with propagators as those obtained for the case $(\Phi, \Phi') = (H^-, \Phi^0)$, except for

$$iT_5^{\{\lambda\}} = D_d(p_3 - p_2)D_u(p_1 - p_4)M_5^{\{\lambda\}}, \quad (71)$$

and with spinor functions as in eqs. (65), for $i = 1, 4, 5$, where

$$\begin{aligned} (c_{R_{\Phi^0}}^q, c_{L_{\Phi^0}}^q) &\rightarrow (c_{L_{H^\pm}}, c_{R_{H^\pm}}), & q = u, d, \\ (c_{R_\gamma}^u, c_{L_\gamma}^u) &\rightarrow (c_{R_\gamma}^d, c_{L_\gamma}^d), & \text{in } M_5^{\{\lambda\}}. \end{aligned} \quad (72)$$

We give explicitly the remaining $T_i^{\{\lambda\}}$'s and $M_i^{\{\lambda\}}$'s, for $i = 7, \dots, 17$. They are

$$\begin{aligned} iT_7^{\{\lambda\}} &= D_d(p_1 + p_2)(D_\gamma(p_4 + p_5)M_{7,\gamma}^{\{\lambda\}}\mathcal{H}_{7,\gamma} + D_{Z^0}(p_4 + p_5)M_{7,Z^0}^{\{\lambda\}}\mathcal{H}_{7,Z^0}), \\ iT_8^{\{\lambda\}} &= D_d(p_3 - p_2)(D_\gamma(p_4 + p_5)M_{8,\gamma}^{\{\lambda\}}\mathcal{H}_{8,\gamma} + D_{Z^0}(p_4 + p_5)M_{8,Z^0}^{\{\lambda\}}\mathcal{H}_{8,Z^0}), \\ iT_9^{\{\lambda\}} &= D_d(p_1 + p_2)(D_{H^0}(p_4 + p_5)M_{9,H^0}^{\{\lambda\}}\mathcal{H}_{9,H^0} + D_{h^0}(p_4 + p_5)M_{9,h^0}^{\{\lambda\}}\mathcal{H}_{9,h^0}), \\ iT_{10}^{\{\lambda\}} &= D_d(p_3 - p_2)(D_{H^0}(p_4 + p_5)M_{10,H^0}^{\{\lambda\}}\mathcal{H}_{10,H^0} + D_{h^0}(p_4 + p_5)M_{10,h^0}^{\{\lambda\}}\mathcal{H}_{10,h^0}), \\ iT_{11}^{\{\lambda\}} &= -D_{H^\pm}(p_2 - p_4)D_u(p_3 + p_5)M_{11}^{\{\lambda\}}\mathcal{H}_{11}, & iT_{12}^{\{\lambda\}} &= D_{H^\pm}(p_2 - p_5)D_d(p_1 - p_4)M_{12}^{\{\lambda\}}\mathcal{H}_{12}, \\ iT_{13}^{\{\lambda\}} &= -D_{H^\pm}(p_2 - p_5)(D_{H^0}(p_1 - p_3)M_{13,H^0}^{\{\lambda\}}\mathcal{H}_{13,H^0} + D_{h^0}(p_1 - p_3)M_{13,h^0}^{\{\lambda\}}\mathcal{H}_{13,h^0}), \\ iT_{14}^{\{\lambda\}} &= D_{H^\pm}(p_2 - p_4)(D_{H^0}(p_1 - p_3)M_{14,H^0}^{\{\lambda\}}\mathcal{H}_{14,H^0} + D_{h^0}(p_1 - p_3)M_{14,h^0}^{\{\lambda\}}\mathcal{H}_{14,h^0}), \\ iT_{15}^{\{\lambda\}} &= -D_{H^\pm}(p_2 - p_5)(D_\gamma(p_1 - p_3)M_{15,\gamma}^{\{\lambda\}}\mathcal{H}_{15,\gamma} + D_{Z^0}(p_1 - p_3)M_{15,Z^0}^{\{\lambda\}}\mathcal{H}_{15,Z^0}), \\ iT_{16}^{\{\lambda\}} &= D_{H^\pm}(p_2 - p_4)(D_\gamma(p_1 - p_3)M_{16,\gamma}^{\{\lambda\}}\mathcal{H}_{16,\gamma} + D_{Z^0}(p_1 - p_3)M_{16,Z^0}^{\{\lambda\}}\mathcal{H}_{16,Z^0}), \end{aligned}$$

$$iT_{17}^{\{\lambda\}} = D_\gamma(p_1 - p_3)M_{17,\gamma}^{\{\lambda\}}\mathcal{H}_{17,\gamma} + D_{Z^0}(p_1 - p_3)M_{17,Z^0}^{\{\lambda\}}\mathcal{H}_{17,Z^0}, \quad (73)$$

and

$$\begin{aligned} M_{7,V}^{\{\lambda\}} &= \sum_{\lambda=\pm} \sum_{\lambda'=\pm} \sum_{i=4,5,6,7} \sum_{j=1,2} (-c_{H^-,H^+;i}^V b_j) Y([3]; [i]; 1, 1) Y([i]; [j]; c_{R_V}^d, c_{L_V}^d) \\ &\quad \times Z([j]; [1]; [2]; (2); c_{R_\gamma}^d, c_{L_\gamma}^d; 1, 1), \\ M_{8,V}^{\{\lambda\}} &= \sum_{\lambda=\pm} \sum_{\lambda'=\pm} \sum_{i=2,3} \sum_{j=4,5,6,7} (b_i c_{H^-,H^+;j}^V) Z([3]; [i]; [2]; (2); c_{R_\gamma}^d, c_{L_\gamma}^d; 1, 1) \\ &\quad \times Y([i]; [j]; 1, 1) Y([j]; [1]; c_{R_V}^d, c_{L_V}^d), \\ M_{9,S}^{\{\lambda\}} &= \sum_{\lambda=\pm} \sum_{i=1,2} (-b_i) Y([3]; [i]; c_{R_S}^d, c_{L_S}^d) Z([i]; [1]; [2]; (2); c_{R_\gamma}^d, c_{L_\gamma}^d; 1, 1), \\ M_{10,S}^{\{\lambda\}} &= \sum_{\lambda=\pm} \sum_{i=2,3} (b_i) Z([3]; [i]; [2]; (2); c_{R_\gamma}^u, c_{L_\gamma}^u; 1, 1) Y([i]; [1]; c_{R_S}^d, c_{L_S}^d), \\ M_{11}^{\{\lambda\}} &= \sum_{\lambda=\pm} \sum_{i=3,5,7} (b_i) (-2\mathcal{Y}_2) Y([3]; [i]; c_{L_{H^\pm}}, c_{R_{H^\pm}}) Y([i]; [1]; c_{R_{H^\pm}}, c_{L_{H^\pm}}), \\ M_{12}^{\{\lambda\}} &= \sum_{\lambda=\pm} \sum_{i=1,4,6} (-b_i) (-2\mathcal{Y}'_2) Y([3]; [i]; c_{L_{H^\pm}}, c_{R_{H^\pm}}) Y([i]; [1]; c_{R_{H^\pm}}, c_{L_{H^\pm}}), \\ M_{13}^{\{\lambda\}} &= (-2\mathcal{Y}'_2) [Y([3]; [1]; c_{R_S}^d, c_{L_S}^d)], \\ M_{14}^{\{\lambda\}} &= (-2\mathcal{Y}_2) [Y([3]; [1]; c_{R_S}^d, c_{L_S}^d)], \\ M_{15,\gamma}^{\{\lambda\}} &= (-2\mathcal{Y}'_2) [\mathcal{F}_{31}^\gamma - 2\mathcal{X}_{31}^\gamma], \\ M_{15,Z^0}^{\{\lambda\}} &= (-2\mathcal{Y}'_2) [\mathcal{F}_{31}^{Z^0} - 2\mathcal{X}_{31}^{Z^0} - \frac{(p_1 - p_3) \cdot (p_1 - p_3 - 2p_4)}{M_{Z^0}^2} \mathcal{F}_{31}^{Z^0}], \\ M_{16,\gamma}^{\{\lambda\}} &= (-2\mathcal{Y}_2) [\mathcal{F}_{31}^\gamma - 2\mathcal{X}_{31}^{\gamma'}], \\ M_{16,Z^0}^{\{\lambda\}} &= (-2\mathcal{Y}_2) [\mathcal{F}_{31}^{Z^0} - 2\mathcal{X}_{31}^{Z^0} - \frac{(p_1 - p_3) \cdot (p_1 - p_3 - 2p_5)}{M_{Z^0}^2} \mathcal{F}_{31}^{Z^0}], \\ M_{17,\gamma}^{\{\lambda\}} &= \tilde{\mathcal{Z}}_{312}^{d\gamma}, \\ M_{17,Z^0}^{\{\lambda\}} &= \tilde{\mathcal{Z}}_{312}^{dZ^0} - \frac{\mathcal{F}_{31}^{Z^0} \mathcal{X}_2}{M_{Z^0}^2}. \end{aligned} \quad (74)$$

6. Process $g\gamma \rightarrow u\bar{d}H^-$.

The Feynman diagrams for

$$g(p_1, \lambda_1) + \gamma(p_2, \lambda_2) \longrightarrow u(p_3, \lambda_3) + \bar{d}(p_4, \lambda_4) + H^-(p_5), \quad (75)$$

are shown in fig. 3, where

$$q = u \quad q' = d, \quad \Phi = H^-, \quad S^* = H^{\pm*}, \quad (76)$$

The amplitude squared is

$$|\overline{M}| = \frac{e^4 g_s^2}{4} N_1^2 N_2^2 \sum_{\{\lambda\}} \sum_{l,m=1}^8 T_l^{\{\lambda\}} T_m^{\{\lambda\}*}. \quad (77)$$

The expressions for the $T_i^{\{\lambda\}}$'s are

$$\begin{aligned} -iT_1^{\{\lambda\}} &= D_d(p_3 + p_5) D_d(p_1 - p_4) M_1^{\{\lambda\}} \mathcal{H}_1, & -iT_2^{\{\lambda\}} &= D_u(p_3 - p_2) D_d(p_1 - p_4) M_2^{\{\lambda\}} \mathcal{H}_2, \\ -iT_3^{\{\lambda\}} &= D_u(p_3 - p_2) D_u(p_4 + p_5) M_3^{\{\lambda\}} \mathcal{H}_3, \\ -iT_{i+3}^{\{\lambda\}} &= -iT_i^{\{\lambda\}}(u \leftrightarrow d; p_3 \leftrightarrow p_4), & i &= 1, \dots, 3, \\ -iT_7^{\{\lambda\}} &= D_{H^\pm}(p_2 - p_5) D_d(p_1 - p_4) M_7^{\{\lambda\}} \mathcal{H}_7, & -iT_8^{\{\lambda\}} &= -iT_7^{\{\lambda\}}(u \leftrightarrow d; p_3 \leftrightarrow p_4), \end{aligned} \quad (78)$$

while the spinor functions are

$$\begin{aligned} M_1^{\{\lambda\}} &= \sum_{\lambda=\pm} \sum_{\lambda'=\pm} \sum_{i=3,5,7} \sum_{j=1,4} (-b_i b_j) Y([3]; [i]; c_{R_{H^\pm}}, c_{L_{H^\pm}}) \\ &\quad \times Z([i]; [j]; [2]; (2); c_{R_\gamma}^d, c_{L_\gamma}^d; 1, 1) Z([j]; [4]; [1]; (1); c_{R_g}^d, c_{L_g}^d; 1, 1), \\ M_2^{\{\lambda\}} &= \sum_{\lambda=\pm} \sum_{\lambda'=\pm} \sum_{i=2,3} \sum_{j=1,4} (-b_i b_j) Z([3]; [i]; [2]; (2); c_{R_\gamma}^u, c_{L_\gamma}^u; 1, 1) \\ &\quad \times Y([i]; [j]; c_{R_{H^\pm}}, c_{L_{H^\pm}}) Z([j]; [4]; [1]; (1); c_{R_g}^d, c_{L_g}^d; 1, 1), \\ M_3^{\{\lambda\}} &= \sum_{\lambda=\pm} \sum_{\lambda'=\pm} \sum_{i=2,3} \sum_{j=4,5,7} (-b_i b_j) Z([3]; [i]; [2]; (2); c_{R_\gamma}^u, c_{L_\gamma}^u; 1, 1) \\ &\quad \times Z([i]; [j]; [1]; (1); c_{R_g}^u, c_{L_g}^u; 1, 1) Y([j]; [4]; c_{R_{H^\pm}}, c_{L_{H^\pm}}), \\ M_{i+3}^{\{\lambda\}} &= M_i^{\{\lambda\}}(u \leftrightarrow d; p_3 \leftrightarrow p_4), & i &= 1, \dots, 3, \\ M_7^{\{\lambda\}} &= \sum_{\lambda=\pm} \sum_{\lambda'=\pm} \sum_{i=1,4} (-b_i) (-2\mathcal{Y}'_2) Y([3]; [i]; c_{R_{H^\pm}}, c_{L_{H^\pm}}) Z([i]; [4]; [1]; (1); c_{R_g}^d, c_{L_g}^d; 1, 1) \\ M_8^{\{\lambda\}} &= -M_7^{\{\lambda\}}(u \leftrightarrow d; p_3 \leftrightarrow p_4). \end{aligned} \quad (79)$$

7. Process $g\gamma \rightarrow u\bar{u}\Phi^0$.

The Feynman diagrams for

$$g(p_1, \lambda_1) + \gamma(p_2, \lambda_2) \longrightarrow u(p_3, \lambda_3) + \bar{u}(p_4, \lambda_4) + \Phi^0(p_5), \quad (80)$$

with $\Phi^0 = H^0, h^0$ or A^0 , can be obtained from fig. 3 by

$$\begin{aligned} q &= q' = u, & \Phi &= \Phi^0, \\ M_i^{\{\lambda\}} &= 0, & i &= 7, 8. \end{aligned} \quad (81)$$

With the exchanges

$$d \rightarrow u, \quad H^\pm \rightarrow \Phi^0, \quad (c_{R_{H^\pm}}, c_{L_{H^\pm}}) \rightarrow (c_{R_{\Phi^0}}^u, c_{L_{\Phi^0}}^u), \quad (82)$$

in eqs. (78)–(79), the expressions for $T_i^{\{\lambda\}}$ and $M_i^{\{\lambda\}}$ ($i = 1, \dots, 6$) can be easily obtained, while eq. (77) remains the same.

By trivial relabeling and sign exchanges, it is possible to obtain from the above formulae the corresponding ones for the u -type quark initiated processes

$$\begin{aligned} u\gamma &\rightarrow dW^+\Phi^0, \\ u\gamma &\rightarrow uZ^0\Phi^0, \\ u\gamma &\rightarrow dH^+\Phi^0, \\ u\gamma &\rightarrow u\Phi^0\Phi^{0'}, \\ u\gamma &\rightarrow uH^+H^-, \end{aligned} \quad (83)$$

as for the charge conjugate reactions

$$\begin{aligned} \bar{d}\gamma &\rightarrow \bar{u}W^+\Phi^0, \\ \bar{d}\gamma &\rightarrow \bar{d}Z^0\Phi^0, \\ \bar{d}\gamma &\rightarrow \bar{u}H^+\Phi^0, \\ \bar{d}\gamma &\rightarrow \bar{d}\Phi^0\Phi^{0'}, \\ \bar{d}\gamma &\rightarrow \bar{d}H^+H^-, \end{aligned} \quad (84)$$

and

$$\begin{aligned} \bar{u}\gamma &\rightarrow \bar{d}W^-\Phi^0, \\ \bar{u}\gamma &\rightarrow \bar{u}Z^0\Phi^0, \\ \bar{u}\gamma &\rightarrow \bar{d}H^-\Phi^0, \\ \bar{u}\gamma &\rightarrow \bar{u}\Phi^0\Phi^{0'}, \\ \bar{u}\gamma &\rightarrow \bar{u}H^-H^+. \end{aligned} \quad (85)$$

Finally, the same it can be done for obtaining the helicity amplitudes for the g -initiated processes

$$\begin{aligned} g\gamma &\rightarrow d\bar{u}H^+, \\ g\gamma &\rightarrow d\bar{d}\Phi^0. \end{aligned} \quad (86)$$

References

- [1] S.L. Glashow, *Nucl. Phys.* **22** (1961) 579;
S. Weinberg, *Phys. Rev. Lett.* **19** (1967) 1264;
A. Salam, Proceedings of the “*Nobel Symposium*”, ed. N. Svartholm, Almqvist and Wiksells, Stockholm, 1968, 367;
P.W. Higgs, *Phys. Rev. Lett.* **12** (1964) 132.
- [2] For a review, see for example:
M.S. Chanowitz, *Ann. Rev. Nucl. Part. Phys.* **38** (1988) 323, and references therein;
M. Sher, *Phys. Rep.* **179** (1989) 273, and references therein;
R.N. Chan, in Proceedings of the “*1990 Gif Summer School of Particle Physics*”, Strasbourg, France, 3–7
September, 1990, and references therein;
G. Altarelli, in Proceedings of “*XXVIth Rencontre de Moriond, Electroweak Interactions and Unified Theories*”, Les Arcs, Savoie, France, March 11–17, 1991, ed. J. Trân Thanh Vân, and references therein.
- [3] For a review, see for example:
H.P. Nilles, *Phys. Rep.* **110** (1984) 1, and references therein;
H.E. Haber and G.L. Kane, *Phys. Rep.* **117** (1985) 75, and references therein;
R. Barbieri, *Riv. Nuovo Cimento* **11** (1988) 1, and references therein.
- [4] G.G. Ross, in Proceedings of “*Joint International Lepton-Hadron Symposium and Eu-rophysics Conference on High Energy Physics*”, Geneva, Switzerland, 25 July–1 August, 1992, eds. S. Hegarty *et al.*, Vol. I, and references therein.
- [5] ALEPH Coll., “*Searches for non-standard neutral Higgs bosons*”, ALEPH note 93–51, March 1993;
D. Treille, Talk given at the “*II Workshop on Physics and Experiments with e^+e^- Col-liders*”, April 1993, Waikoloa, Hawaii.
- [6] J.F. Gunion, H.E. Haber, G.L. Kane and S. Dawson, “*The Higgs Hunter Guide*” (Addison-Wesley, Reading MA, 1990).
- [7] P. Langacker and H.A. Weldon, *Phys. Rev. Lett.* **52** (1984) 1377;
H.A. Weldon, *Phys. Rev.* **D30** (1984) 1547; *Phys. Lett.* **B146** (1984) 59.
- [8] R. Casalbuoni, D. Dominici, F. Feruglio and R. Gatto, *Nucl. Phys.* **B299** (1988) 117.
- [9] Proceedings of the “*Large Hadron Collider Workshop*”, Aachen, 4–9 October 1990, eds. G. Jarlskog and D. Rein, Report CERN 90–10, ECFA 90–133, Geneva, 1990.
- [10] Proceedings of the “*Summer Study on High Energy Physics in the 1990s*”, ed. S. Jensen, Snowmass, Colorado, 1988;
Proceedings of the “*1990 Summer Study on High Energy Physics: Research Directions for the Decade*”, ed. E.L. Berger, Snowmass, Colorado, 1990.

- [11] Proceedings of the “*ECFA workshop on LEP 200*”,
A. Bohm and W. Hoogland eds., Aachen FRG, 29 Sept.–1 Oct. 1986, CERN 87-08.
- [12] Proceedings of the Workshop “*Physics and Experiments with Linear Colliders*”, Saariselkä, Finland, 9–14 September 1991,
eds. R. Orawa, P. Eerola and M. Nordberg, World Scientific Publishing, Singapore, 1992.
- [13] Proceedings of the Workshop “ *e^+e^- Collisions at 500 GeV. The Physics Potential*”, Munich, Annecy, Hamburg, 3–4 February 1991, ed. P.M. Zerwas, DESY pub. 92–123A/B/C, August 1992.
- [14] Proceedings of the ECFA workshop on “ *e^+e^- Linear Colliders LC92*”, R. Settles ed., Garmisch Partenkirchen, 25 July–2 Aug. 1992, MPI-PhE/93–14, ECFA 93–154.
- [15] Proceedings of the “*I Workshop on Japan Linear Collider (JLC)*”, KEK 1989, KEK-Report 90–2;
Proceedings of the “*II Workshop on Japan Linear Collider (JLC)*”, KEK 1990, KEK-Report 91–10.
- [16] J. Gunion, L. Roszkowski, A. Turski, H. Haber, G. Gamberini, B. Kayser, S. Novaes, F. Olness and J. Wudka, *Phys. Rev.* **D38** (1988) 3444.
- [17] J. Dai, J.F. Gunion and R. Vega, *Phys. Lett.* **B315** (1993) 355.
- [18] *Solenoidal Detector Collaboration Technical Design Report*, E.L. Berger *et al.*, Report SDC–92–201, SSCL–SR–1215, 1992.
- [19] A. Ballestrero, E. Maina, S. Moretti and C. Pistarino, *Phys. Lett.* **B320** (1994) 305.
- [20] Z. Kunszt and F. Zwirner, *Nucl. Phys.* **B385** (1992) 3, and references therein.
- [21] A. Djouadi, J. Kalinowski and P.M. Zerwas, in ref. [13].
- [22] S. Komamiya, *Phys. Rev.* **D38** (1988) 2158.
- [23] A. Djouadi, D. Haidt and P.M. Zerwas, in ref. [13].
- [24] P.R. Burchat, D.L. Burke and A. Petersen, *Phys. Rev.* **D38** (1988) 2735;
Errata *Phys. Rev.* **D39** (1989) 3515.
- [25] J.F. Gunion and H.E. Haber, *preprint* UCD–90–25, September 1990, presented in “*1990 DPF Summer Study on High Energy Physics*”, Snowmass, Colorado, June 25–July 13, 1990;
J.F. Gunion and H.E. Haber, in ref. [10] (1990);
J.F. Gunion and H.E. Haber, *Phys. Rev.* **D48** (1993) 5109.
- [26] J.F. Gunion, *preprint* UCD–92–27, November 1992, to be published in the Proceeding of “*Particles and Fields 92: 7th Meeting of the Division of Particle Fields of the APS (DPF 92)*”, Batavia, Illinois, 10–14 November 1992;
J.F. Gunion, *preprint* UCD–93–8, February 1993.

- [27] D. Bowser-Chao, K. Cheung and S. Thomas, *Phys. Lett.* **B315** (1993) 399.
- [28] S. Moretti, *Phys. Rev.* **D50** (1994) 2016.
- [29] Proceedings of the “*HERA Workshop*”, ed. R.D. Peccei, Desy, Hamburg, October 1987; Proceedings of the “*HERA Workshop*”, eds. W. Buchmüller and G. Ingelman, Desy, Hamburg, October 1991.
- [30] K.J.F. Gaemers, R.M. Godbole and M. van der Horst, in ref. [29] (1987).
- [31] R. Bates and J.N. Ng, *Phys. Rev.* **D33** (1986) 657.
- [32] I.S. Choi, B.H. Cho, B.R. Kim and R. Rodenberg, *Phys. Lett.* **B200** (1988) 200.
- [33] B. Grzadkowski and W.-S. Hou, *Phys. Lett.* **B210** (1988) 233.
- [34] T. Han and C. Liu, *Z. Phys.* **C28** (1985) 295.
- [35] B. Grzadkowski, S. Pokorski and J. Rosiek, *Phys. Lett.* **B272** (1991) 143.
- [36] K. Hikasa, Particle Data Book, *Phys. Rev.* **D45** 11-II (1992).
- [37] G. Grindhammer, D. Haidt, J. Ohnemus, J. Vermaseren and D. Zeppenfeld, in ref. [9].
- [38] D.A. Dicus and S. Willenbrock, *Phys. Rev.* **D32** (1985) 1642.
- [39] J. Blumlein, G.J. van Oldenborgh and R. Ruckl, *Nucl. Phys.* **B395** (1993) 35.
- [40] J.L Diaz-Cruz and O.A. Sampayo, *Barcelona Autonomo University preprint* UAB-FT-286-92, May 1992.
- [41] K. Cheung, *Phys. Lett.* **B319** (1993) 244.
- [42] R. Kleiss and W.J. Stirling, *Nucl. Phys.* **B262** (1985) 235.
- [43] C. Mana and M. Martinez, *Nucl. Phys.* **B287** (1987) 601.
- [44] K. Hagiwara and D. Zeppenfeld, *Nucl. Phys.* **B274** (1986) 1.
- [45] A.D. Martin, R.G. Roberts and W.J. Stirling, *Phys. Rev.* **D50** (1994) 6734.
- [46] V. Telnov, *Nucl. Instrum. Methods* **A294** (1990) 72;
I. Ginzburg, G. Kotkin, V. Serbo and V. Telnov, *Nucl. Instrum. Methods* **A205** (1983) 47, **A219** (1984) 5.
- [47] G.P. Lepage, *Jour. Comp. Phys.* **27** (1978) 192.
- [48] G. Abu Leil and S. Moretti, *preprint* DFTT 26/94, DTP/94/46, December 1994, revised July 1995.

- [49] Y. Okada, M. Yamaguchi and T. Yanagida, *Prog. Teor. Phys. Lett.* **85** (1991) 1;
 J. Ellis, G. Ridolfi and F. Zwirner, *Phys. Lett.* **B257** (1991) 83; *Phys. Lett.* **B262** (1991) 477;
 H.E. Haber and R. Hempfling, *Phys. Rev. Lett.* **66** (1991) 1815;
 R. Barbieri and M. Frigeni, *Phys. Lett.* **B258** (1991) 395.
- [50] A. Brignole, J. Ellis, G. Ridolfi and F. Zwirner, *Phys. Lett.* **B271** (1991) 123;
 A. Brignole, *Phys. Lett.* **B277** (1992) 313.
- [51] V. Barger, K. Cheung, R.J. Phillips and A.L. Stange, *Phys. Rev.* **D46** (1992) 4914.
- [52] CDF Collaboration, F. Abe *et al.*, *Phys. Rev.* **D50** (1994) 2966; *Phys. Rev. Lett.* **73** (1994) 225; *preprint* FERMILAB-PUB-94/022-E,CDF/PUB/TOP/PUBLIC/3040, March 1995.
- [53] G.L. Kane, Proceedings of the “*Madison Workshop*” (1979).
- [54] J.H. Kühn, *Act. Phys. Pol.* **B12** (1981) 347;
 J.H. Kühn, *Act. Phys. Austr. Suppl.* **XXIV** (1982) 203.
- [55] S. Moretti and W.J. Stirling, *Phys. Lett.* **B347** (1995) 291.
- [56] See, for example:
 Proceedings of the “*High Luminosities at LEP*” Workshop, CERN Report 91-02, eds. E. Blucher *et al.*
- [57] T. Stelzer and W.F. Long, *Comp. Phys. Comm.* **81** (1994) 357;
 E. Murayama, I. Watanabe and K. Hagiwara, HELAS: HELicity Amplitude Subroutines for Feynman Diagram Evaluations, *KEK Report* 91-11, January 1992.
- [58] K. Cheung, *Phys. Rev.* **D48** (1993) 1035.
- [59] ATLAS Technical Proposal, CERN/LHC/94-43 LHCC/P2, December 1994.
- [60] CMS Technical Proposal, CERN/LHC/94-43 LHCC/P1, December 1994.

Table Captions

table I Cross sections of the processes $q\gamma \rightarrow q'W^\pm\Phi^0$, where $\Phi^0 = H^0, h^0, A^0$, at $\sqrt{s}_{ep} = 1.36$ TeV, for $M_{A^0} = 60, 80, 100, 120, 140$ GeV, with $\tan\beta = 1.5$ (a) and 30 (b). The MRS(A) structure functions are used. The errors are the statistical errors on the numerical calculation. Entries are in GeV for masses, and in fb for cross sections.

table II Cross sections of the processes $q\gamma \rightarrow qZ^0\Phi^0$, where $\Phi^0 = H^0, h^0, A^0$, at $\sqrt{s}_{ep} = 1.36$ TeV, for $M_{A^0} = 60, 80, 100, 120, 140$ GeV, with $\tan\beta = 1.5$ (a) and 30 (b). The MRS(A) structure functions are used. The errors are the statistical errors on the numerical calculation. Entries are in GeV for masses, and in fb for cross sections.

table III Cross sections of the processes $q\gamma \rightarrow q'H^\pm\Phi^0$, where $\Phi^0 = H^0, h^0, A^0$, at $\sqrt{s}_{ep} = 1.36$ TeV, for $M_{A^0} = 60, 80, 100, 120, 140$ GeV, with $\tan\beta = 1.5$ (a) and 30 (b). The MRS(A) structure functions are used. The errors are the statistical errors on the numerical calculation. Entries are in GeV for masses, and in fb for cross sections.

table IV Cross sections of the processes $q\gamma \rightarrow q\Phi^0\Phi^{0'}$, where $(\Phi^0, \Phi^{0'}) = (H^0, A^0), (h^0, A^0)$, at $\sqrt{s}_{ep} = 1.36$ TeV, for $M_{A^0} = 60, 80, 100, 120, 140$ GeV, with $\tan\beta = 1.5$ (a) and 30 (b). The MRS(A) structure functions are used. The errors are the statistical errors on the numerical calculation. Entries are in GeV for masses, and in fb for cross sections.

table V Cross sections of the process $q\gamma \rightarrow qH^+H^-$, at $\sqrt{s}_{ep} = 1.36$ TeV, for $M_{A^0} = 60, 80, 100, 120, 140$ GeV, with $\tan\beta = 1.5$ (a) and 30 (b). The MRS(A) structure functions are used. The errors are the statistical errors on the numerical calculation. Entries are in GeV for masses, and in fb for cross sections.

table VI Cross sections of the process $g\gamma \rightarrow q\bar{q}'H^\pm$, at $\sqrt{s}_{ep} = 1.36$ TeV, for $M_{A^0} = 60, 80, 100, 120, 140$ GeV, with $\tan\beta = 1.5$ (a) and 30 (b). The MRS(A) structure functions are used. The errors are the statistical errors on the numerical calculation. Entries are in GeV for masses, and in fb for cross sections.

table VII Cross sections of the processes $g\gamma \rightarrow q\bar{q}\Phi^0$, where $\Phi^0 = H^0, h^0, A^0$, at $\sqrt{s}_{ep} = 1.36$ TeV, for $M_{A^0} = 60, 80, 100, 120, 140$ GeV, with $\tan\beta = 1.5$ (a) and 30 (b). The MRS(A) structure functions are used. The errors are the statistical errors on the numerical calculation. Entries are in GeV for masses, and in fb for cross sections.

table VIII Production cross sections for the discrete and continuum background processes discussed in the text. Case (a) contains the cross sections which do not have dependence on the $MSSM$ parameters, whereas (b) shows the case in which resonant t -quarks introduce such a dependence through Γ_t^{MSSM} . In (b) the five entries for each process correspond to the five different values of $M_{A^0} = 60, 80, 100, 120$ and 140 GeV. Numbers in brackets are for the case $\tan\beta = 30$. The MRS(A) structure functions are used. The errors are the statistical errors on the numerical calculation. Entries are in GeV for masses, and in fb for cross sections.

table IX Total top width and BRs of the decay channels $t \rightarrow bW^\pm$ and $t \rightarrow bH^\pm$ within the $MSSM$, for $\tan\beta = 1.5$ and 30, for the different values of M_{H^\pm} corresponding to

$M_{A^0} = 60, 80, 100, 120$ and 140 GeV. The total top width in the \mathcal{SM} is $\Gamma_t^{\mathcal{SM}} \approx 1.57$ GeV. Entries are in GeV both for masses and widths.

table A.I Neutral \mathcal{MSSM} Higgs boson couplings each other, to the gauge bosons W^\pm , Z^0 and γ , and to the \mathcal{MSSM} H^\pm 's.

table A.II Charged \mathcal{MSSM} Higgs boson couplings to the gauge bosons Z^0 and γ (here $c_{2W} \equiv \cos 2\theta_W$).

table A.III \mathcal{MSSM} right and left handed couplings (c_R, c_L) of u - (upper line) and d -type (lower line) quarks to the neutral gauge bosons g, γ, Z^0 and to the neutral \mathcal{MSSM} Higgses H^0, h^0, A^0 . We have $g_R^q = -Q^q s_W^2$ and $g_L^q = T_3^q - Q^q s_W^2$ ($q = u, d$), with $(Q^u, T_3^u) = (+\frac{2}{3}, \frac{1}{2})$ and $(Q^d, T_3^d) = (-\frac{1}{3}, -\frac{1}{2})$ for quark charges and isospins.

table A.IV \mathcal{MSSM} right and left handed couplings (c_R, c_L) of quarks to the charged gauge bosons W^\pm and to the charged \mathcal{MSSM} Higgses H^\pm .

Figure Captions

fig. 1 Feynman diagrams contributing in the lowest order to $q\gamma \rightarrow q'V\Phi^0$, where $q(q')$ represents a quark, $V(V^*)$ an external(internal) vector boson, S^* an internal scalar Higgs boson and Φ^0 one of the neutral \mathcal{MSSM} Higgses, in the unitary gauge. For the possible combinations of $(q, q', V, V^*, S^*, \Phi^0)$ and the corresponding non-vanishing graphs, see the text.

fig. 2 Feynman diagrams contributing in the lowest order to $q\gamma \rightarrow q'\Phi\Phi'$, where $q(q')$ represents a quark, V^* an internal vector boson, S^* and $S^{*'}$ internal scalar Higgs bosons and Φ and Φ' both neutral and charged \mathcal{MSSM} Higgses, in the unitary gauge. For the possible combinations of $(q, q', V^*, S^*, S^{*'}, \Phi, \Phi')$ and the corresponding non-vanishing graphs, see the text.

fig. 3 Feynman diagrams contributing in the lowest order to $g\gamma \rightarrow q\bar{q}'\Phi$, where $q(q')$ represents a quark, S^* an internal scalar Higgs bosons and Φ both neutral and charged \mathcal{MSSM} Higgses, in the unitary gauge. For the possible combinations of (q, q', S^*, Φ) and the corresponding non-vanishing graphs, see the text.

$\sigma(q\gamma \rightarrow q'W^\pm\Phi^0)$					
M_{H^0}	M_{h^0}	M_{A^0}	H^0	h^0	A^0
144.4	56.0	60	7.582 ± 0.024	37.30 ± 0.16	0.25820 ± 0.00090
150.7	63.7	80	5.767 ± 0.019	36.76 ± 0.19	0.18718 ± 0.00058
159.3	70.6	100	3.986 ± 0.011	36.80 ± 0.17	0.13096 ± 0.00043
170.1	76.4	120	2.5569 ± 0.0069	37.02 ± 0.14	0.09185 ± 0.00030
182.9	80.9	140	1.5431 ± 0.0045	37.44 ± 0.14	0.06441 ± 0.00020
$\sqrt{s} = 1.36 \text{ TeV}$			$\tan \beta = 1.5$		MRS(A)

Table Ia

$\sigma(q\gamma \rightarrow q'W^\pm\Phi^0)$					
M_{H^0}	M_{h^0}	M_{A^0}	H^0	h^0	A^0
129.2	59.9	60	24.060 ± 0.074	0.8430 ± 0.0018	1.5041 ± 0.0044
129.2	79.9	80	23.959 ± 0.075	0.6993 ± 0.0015	0.9990 ± 0.0026
129.4	99.7	100	23.692 ± 0.074	0.8049 ± 0.0019	0.6780 ± 0.0016
130.0	119.0	120	21.485 ± 0.067	2.9355 ± 0.0087	0.4636 ± 0.0012
140.9	128.1	140	1.4487 ± 0.0042	22.964 ± 0.070	0.31958 ± 0.00076
$\sqrt{s} = 1.36 \text{ TeV}$			$\tan \beta = 30$		MRS(A)

Table Ib

$\sigma(q\gamma \rightarrow qZ^0\Phi^0)$					
M_{H^0}	M_{h^0}	M_{A^0}	H^0	h^0	A^0
144.4	56.0	60	0.1913 ± 0.0031	4.877 ± 0.050	$(7.962 \pm 0.023) \times 10^{-3}$
150.7	63.7	80	0.1283 ± 0.0014	3.941 ± 0.045	$(5.186 \pm 0.015) \times 10^{-3}$
159.3	70.6	100	0.0803 ± 0.0011	3.260 ± 0.065	$(3.551 \pm 0.010) \times 10^{-3}$
170.1	76.4	120	0.0419 ± 0.0014	2.998 ± 0.037	$(2.4628 \pm 0.0078) \times 10^{-3}$
182.9	80.9	140	0.02421 ± 0.00028	2.705 ± 0.037	$(1.7317 \pm 0.0051) \times 10^{-3}$
$\sqrt{s} = 1.36$ TeV			$\tan \beta = 1.5$		MRS(A)

Table IIa

$\sigma(q\gamma \rightarrow qZ^0\Phi^0)$					
M_{H^0}	M_{h^0}	M_{A^0}	H^0	h^0	A^0
129.2	59.9	60	0.7443 ± 0.0085	1.3557 ± 0.0047	2.2500 ± 0.0080
129.2	79.9	80	0.7406 ± 0.0073	0.9509 ± 0.0032	1.5374 ± 0.0052
129.4	99.7	100	0.7474 ± 0.0078	0.6819 ± 0.0023	1.0753 ± 0.0040
130.0	119.0	120	0.677 ± 0.015	0.5162 ± 0.0022	0.7622 ± 0.0031
140.9	128.1	140	0.3412 ± 0.0011	0.770 ± 0.017	0.5376 ± 0.0018
$\sqrt{s} = 1.36$ TeV			$\tan \beta = 30$		MRS(A)

Table IIb

$\sigma(q\gamma \rightarrow q'H^\pm\Phi^0)$						
M_{H^0}	M_{h^0}	M_{A^0}	M_{H^\pm}	H^0	h^0	A^0
144.4	56.0	60	100.0	0.3621 ± 0.0019	1.1599 ± 0.0085	2.834 ± 0.021
150.7	63.7	80	113.1	0.2683 ± 0.0017	0.5857 ± 0.0037	1.3684 ± 0.0072
159.3	70.6	100	128.1	0.1944 ± 0.0011	0.2866 ± 0.0021	0.6745 ± 0.0037
170.1	76.4	120	144.2	0.1334 ± 0.00081	0.1352 ± 0.0013	0.3518 ± 0.0021
182.9	80.9	140	161.2	0.08182 ± 0.00059	0.06572 ± 0.00031	0.1858 ± 0.0011
$\sqrt{s} = 1.36 \text{ TeV} \quad \tan \beta = 1.5 \quad \text{MRS(A)}$						

Table IIIa

$\sigma(q\gamma \rightarrow q'H^\pm\Phi^0)$						
M_{H^0}	M_{h^0}	M_{A^0}	M_{H^\pm}	H^0	h^0	A^0
129.2	59.9	60	100.0	$(6.833 \pm 0.019) \times 10^{-3}$	2.8210 ± 0.019	2.833 ± 0.020
129.2	79.9	80	113.1	$(6.527 \pm 0.029) \times 10^{-3}$	1.3660 ± 0.0081	1.3697 ± 0.0072
129.4	99.7	100	128.1	$(8.344 \pm 0.044) \times 10^{-3}$	0.6732 ± 0.0056	0.6758 ± 0.0037
130.0	119.0	120	144.2	$(31.52 \pm 0.24) \times 10^{-3}$	0.3224 ± 0.0019	0.3523 ± 0.0021
140.9	128.1	140	161.2	$(171.3 \pm 1.0) \times 10^{-3}$	0.015369 ± 0.000073	0.1860 ± 0.0011
$\sqrt{s} = 1.36 \text{ TeV} \quad \tan \beta = 30 \quad \text{MRS(A)}$						

Table IIIb

$\sigma(q\gamma \rightarrow q\Phi^0\Phi^{0'})$				
M_{H^0}	M_{h^0}	M_{A^0}	$H^0 A^0$	$h^0 A^0$
144.4	56.0	60	0.1468 ± 0.0023	1.0889 ± 0.0092
150.7	63.7	80	0.1004 ± 0.0014	0.3226 ± 0.0041
159.3	70.6	100	0.0715 ± 0.0013	0.1183 ± 0.0018
170.1	76.4	120	0.0409 ± 0.00056	0.0437 ± 0.00075
182.9	80.9	140	0.02656 ± 0.00049	0.0203 ± 0.00025
$\sqrt{s} = 1.36$ TeV			$\tan \beta = 1.5$	MRS(A)

Table IVa

$\sigma(q\gamma \rightarrow q\Phi^0\Phi^{0'})$				
M_{H^0}	M_{h^0}	M_{A^0}	$H^0 A^0$	$h^0 A^0$
129.2	59.9	60	$(6.072 \pm 0.024) \times 10^{-3}$	4.002 ± 0.039
129.2	79.9	80	$(4.279 \pm 0.026) \times 10^{-3}$	1.1668 ± 0.0098
129.4	99.7	100	$(4.489 \pm 0.057) \times 10^{-3}$	0.4270 ± 0.0038
130.0	119.0	120	$(16.05 \pm 0.18) \times 10^{-3}$	0.1746 ± 0.0021
140.9	128.1	140	$(79.9 \pm 1.0) \times 10^{-3}$	0.00802 ± 0.00013
$\sqrt{s} = 1.36$ TeV			$\tan \beta = 30$	MRS(A)

Table IVb

$\sigma(q\gamma \rightarrow qH^+H^-)$	
M_{H^\pm}	H^+H^-
100.0	18.18 ± 0.42
113.1	10.96 ± 0.16
128.1	6.06 ± 0.16
144.2	2.991 ± 0.064
161.2	1.577 ± 0.034
$\sqrt{s} = 1.36 \text{ TeV} \quad \tan \beta = 1.5 \quad \text{MRS(A)}$	

Table Va

$\sigma(q\gamma \rightarrow qH^+H^-)$	
M_{H^\pm}	H^+H^-
100.0	28.13 ± 0.40
113.1	16.52 ± 0.21
128.1	9.52 ± 0.14
144.2	4.244 ± 0.056
161.2	1.867 ± 0.071
$\sqrt{s} = 1.36 \text{ TeV} \quad \tan \beta = 30 \quad \text{MRS(A)}$	

Table Vb

$\sigma(g\gamma \rightarrow q\bar{q}'H^\pm)$	
M_{H^\pm}	H^\pm
100.0	367.3 ± 2.7
113.1	270.5 ± 3.8
128.1	174.3 ± 1.0
144.2	84.78 ± 0.48
161.2	22.78 ± 0.15
$\sqrt{s} = 1.36 \text{ TeV} \quad \tan \beta = 1.5 \quad \text{MRS(A)}$	

Table VIa

$\sigma(g\gamma \rightarrow q\bar{q}'H^\pm)$	
M_{H^\pm}	H^\pm
100.0	621.7 ± 4.8
113.1	460.6 ± 6.0
128.1	291.9 ± 1.7
144.2	142.2 ± 1.7
161.2	40.65 ± 0.31
$\sqrt{s} = 1.36 \text{ TeV} \quad \tan \beta = 30 \quad \text{MRS(A)}$	

Table VIb

$\sigma(g\gamma \rightarrow q\bar{q}\Phi^0)$					
M_{H^0}	M_{h^0}	M_{A^0}	H^0	h^0	A^0
144.4	56.0	60	0.1914 ± 0.0047	2.1015 ± 0.0059	1.4169 ± 0.0041
150.7	63.7	80	0.1541 ± 0.0020	1.6574 ± 0.0051	0.6810 ± 0.0022
159.3	70.6	100	0.1174 ± 0.0029	1.3948 ± 0.0036	0.3640 ± 0.0019
170.1	76.4	120	0.0844 ± 0.0025	1.2121 ± 0.0030	0.2081 ± 0.0010
182.9	80.9	140	0.0588 ± 0.0014	1.1043 ± 0.0025	0.1253 ± 0.00092
$\sqrt{s} = 1.36$ TeV $\tan \beta = 1.5$ MRS(A)					

Table VIIa

$\sigma(g\gamma \rightarrow q\bar{q}\Phi^0)$					
M_{H^0}	M_{h^0}	M_{A^0}	H^0	h^0	A^0
129.2	59.9	60	0.2743 ± 0.0010	428.3 ± 1.7	449.9 ± 1.6
129.2	79.9	80	0.3432 ± 0.0011	209.13 ± 0.83	218.87 ± 0.85
129.4	99.7	100	0.6488 ± 0.0020	115.30 ± 0.55	117.97 ± 0.53
130.0	119.0	120	8.649 ± 0.027	62.86 ± 0.28	67.66 ± 0.31
140.9	128.1	140	36.38 ± 0.17	4.514 ± 0.020	40.76 ± 0.19
$\sqrt{s} = 1.36$ TeV $\tan \beta = 30$ MRS(A)					

Table VIIb

Background	σ
$ep \rightarrow W^\pm Z^0 X$	219.8 ± 3.2
$ep \rightarrow Z^0 Z^0 X$	10.98 ± 0.60
$ep \rightarrow q\bar{q} Z^0 X$	3139 ± 49
$ep \rightarrow W^+ W^- X$	1805 ± 55
$ep \rightarrow q\bar{q}' W^\pm X$	17114 ± 150
$\sqrt{s} = 1.36$ TeV	MRS(A)

Table VIIIa

$W^+ W^- X$ (t -res.)	$tbW^\pm X$	$tbX \rightarrow bbW^+ W^- X$	$t\bar{t}X \rightarrow bbW^+ W^- X$
$809 \pm 20(707 \pm 11)$	$1590.0 \pm 6.6(1406.9 \pm 8.5)$	$291 \pm 16(262 \pm 18)$	$532.6 \pm 2.0(423.4 \pm 1.0)$
$758 \pm 26(704 \pm 11)$	$1586.7 \pm 7.5(1401.8 \pm 6.2)$	$305 \pm 22(280 \pm 20)$	$587.2 \pm 1.0(489.5 \pm 1.1)$
$783 \pm 23(714 \pm 11)$	$1593.6 \pm 6.8(1397.3 \pm 6.3)$	$323 \pm 20(306 \pm 21)$	$656.2 \pm 1.1(579.2 \pm 1.1)$
$783 \pm 22(705 \pm 10)$	$1576.2 \pm 7.8(1401.3 \pm 6.1)$	$341 \pm 34(331 \pm 22)$	$730.2 \pm 1.4(685.6 \pm 1.1)$
$789 \pm 29(708 \pm 11)$	$1569.3 \pm 7.7(1389.8 \pm 6.4)$	$356 \pm 36(352 \pm 26)$	$791.2 \pm 1.0(780.5 \pm 1.2)$
$\sqrt{s} = 1.36$ TeV		$\tan\beta = 1.5(30)$	MRS(A)

Table VIIIb

M_{H^\pm}	$\text{BR}(t \rightarrow bW^\pm)$	$\text{BR}(t \rightarrow bH^\pm)$	Γ_t^{MSSM}
100.0	0.81(0.73)	0.19(0.27)	1.94(2.17)
113.1	0.85(0.78)	0.15(0.22)	1.84(2.02)
128.1	0.90(0.85)	0.10(0.15)	1.75(1.86)
144.2	0.95(0.92)	0.05(0.08)	1.66(1.71)
161.2	0.99(0.98)	0.01(0.02)	1.59(1.60)
$M_{W^\pm} \approx 80 \text{ GeV} \quad \tan \beta = 1.5(30) \quad m_t = 175 \text{ GeV}$			

Table IX

	H^0	h^0	A^0
$W^\pm W^\mp$	$\frac{M_{W^\pm} c_{\beta\alpha}}{s_W}$	$\frac{M_{W^\pm} s_{\beta\alpha}}{s_W}$	0
$H^\pm H^\mp$	$\frac{M_{W^\pm}}{s_W} (c_{\beta\alpha} - \frac{1}{2c_W^2} c_{2\beta} c_{\alpha\beta})$	$\frac{M_{W^\pm}}{s_W} (s_{\beta\alpha} + \frac{1}{2c_W^2} c_{2\beta} s_{\alpha\beta})$	0
$W^\pm H^\mp(\gamma)$	$\frac{s_{\beta\alpha}}{2s_W}$	$-\frac{c_{\beta\alpha}}{2s_W}$	$-\frac{i}{2s_W}$
$Z^0 Z^0$	$\frac{M_{W^\pm}}{s_W c_W^2} c_{\beta\alpha}$	$\frac{M_{W^\pm}}{s_W c_W^2} s_{\beta\alpha}$	0
$Z^0 A^0$	$\frac{i}{2s_W c_W} s_{\beta\alpha}$	$-\frac{1}{2s_W c_W} c_{\beta\alpha}$	0
$H^0 H^0$	$\frac{3M_{W^\pm}}{2s_W c_W^2} c_{2\alpha} c_{\alpha\beta}$	$-\frac{M_{W^\pm}}{2s_W c_W^2} (2s_{2\alpha} c_{\alpha\beta} + c_{2\alpha} s_{\alpha\beta})$	0
$H^0 h^0$	$-\frac{M_{W^\pm}}{2s_W c_W^2} (2s_{2\alpha} c_{\alpha\beta} + c_{2\alpha} s_{\alpha\beta})$	$\frac{M_{W^\pm}}{2s_W c_W^2} (2s_{2\alpha} s_{\alpha\beta} - c_{2\alpha} c_{\alpha\beta})$	0
$H^0 A^0$	0	0	$-\frac{M_{W^\pm}}{2s_W c_W^2} c_{2\beta} c_{\alpha\beta}$
$h^0 h^0$	$\frac{M_{W^\pm}}{2s_W c_W^2} (2s_{2\alpha} s_{\alpha\beta} - c_{2\alpha} c_{\alpha\beta})$	$\frac{3M_{W^\pm}}{2s_W c_W^2} c_{2\alpha} s_{\alpha\beta}$	0
$h^0 A^0$	0	0	$\frac{M_{W^\pm}}{2s_W c_W^2} c_{2\beta} s_{\alpha\beta}$
$A^0 A^0$	$-\frac{M_{W^\pm}}{2s_W c_W^2} c_{2\beta} c_{\alpha\beta}$	$\frac{M_{W^\pm}}{2s_W c_W^2} c_{2\beta} s_{\alpha\beta}$	0

Table A.I

	$H^\pm H^\mp$
γ	1
Z^0	$\frac{1}{2s_W c_W} c_{2W}$
$\gamma\gamma$	-2
γZ^0	$-\frac{c_{2W}}{s_W c_W}$

Table A.II

g	γ	Z^0	H^0	h^0	A^0
(1, 1)	$Q^u(1, 1)$	$\frac{1}{s_W c_W}(g_R^u, g_L^u)$	$\frac{m_u}{2M_{W^\pm} s_W} \frac{s_\alpha}{s_\beta}(1, 1)$	$\frac{m_u}{2M_{W^\pm} s_W} \frac{c_\alpha}{s_\beta}(1, 1)$	$-i \frac{m_u}{2M_{W^\pm} s_W} \frac{1}{t_\beta}(1, -1)$
(1, 1)	$Q^d(1, 1)$	$\frac{1}{s_W c_W}(g_R^d, g_L^d)$	$\frac{m_d}{2M_{W^\pm} s_W} \frac{c_\alpha}{c_\beta}(1, 1)$	$-\frac{m_d}{2M_{W^\pm} s_W} \frac{s_\alpha}{c_\beta}(1, 1)$	$-i \frac{m_d}{2M_{W^\pm} s_W} t_\beta(1, -1)$

Table A.III

W^\pm	H^\pm
$\frac{1}{\sqrt{2}s_W}(0, 1)$	$-\frac{1}{2\sqrt{2}M_{W^\pm} s_W}(m_d t_\beta, m_u/t_\beta)$

Table A.IV

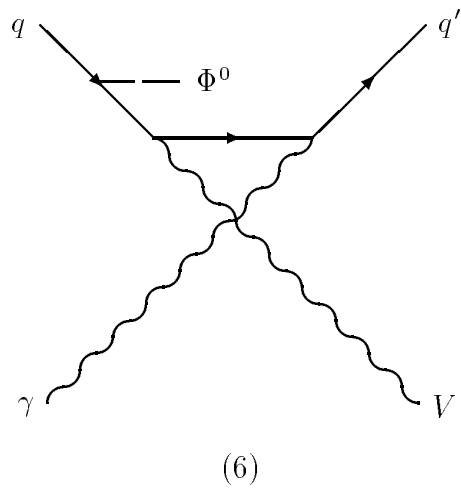
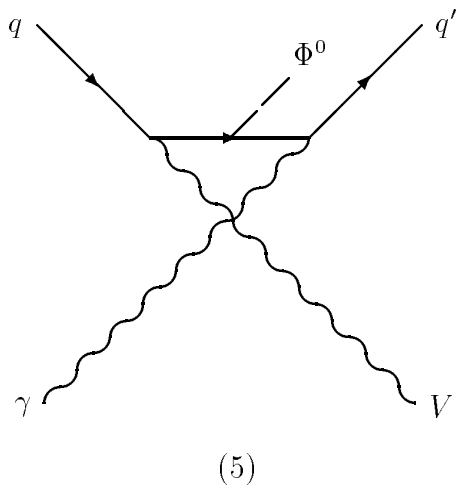
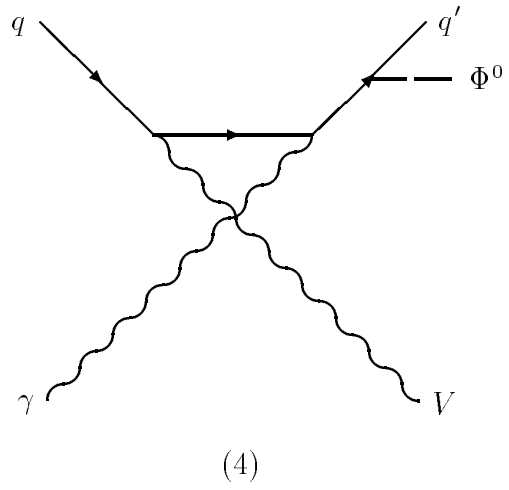
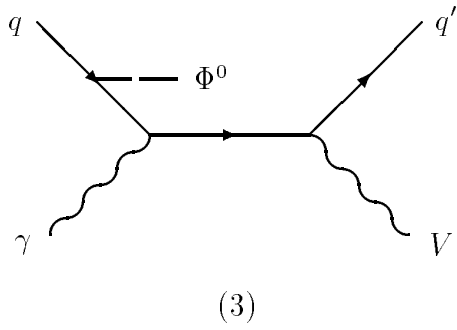
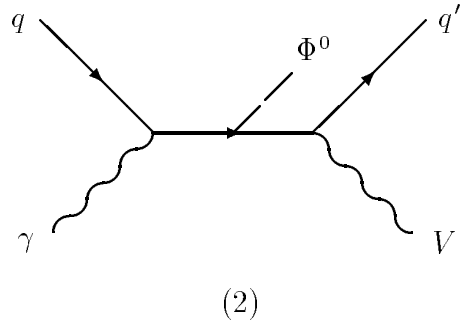
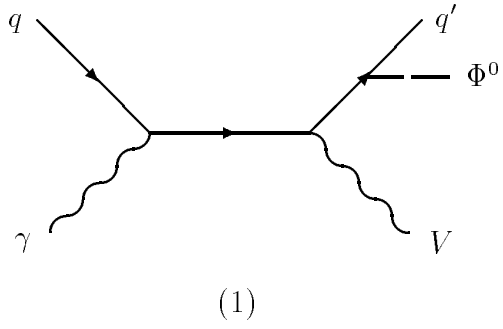


Fig.1

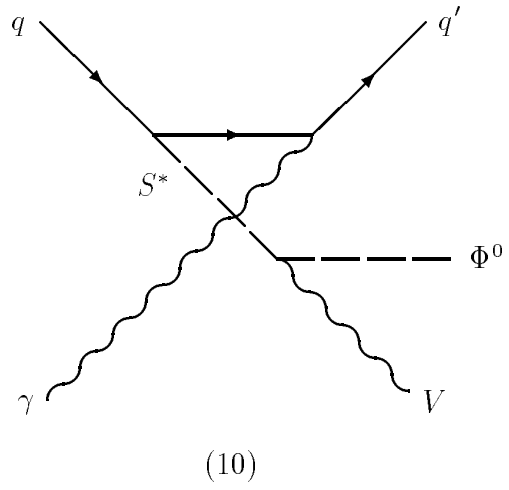
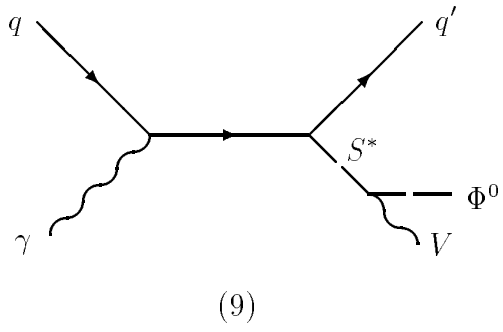
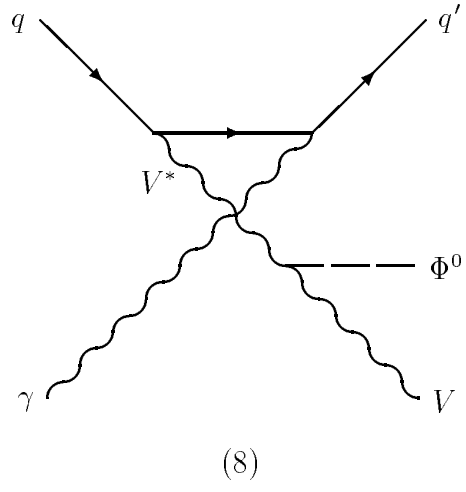
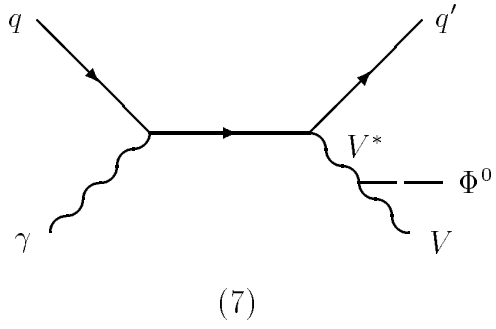


Fig.1 (Continued)

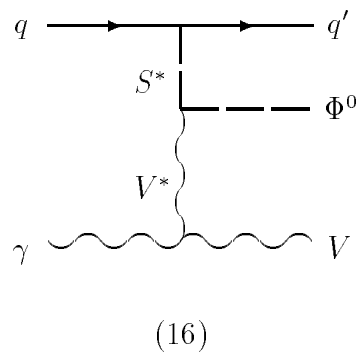
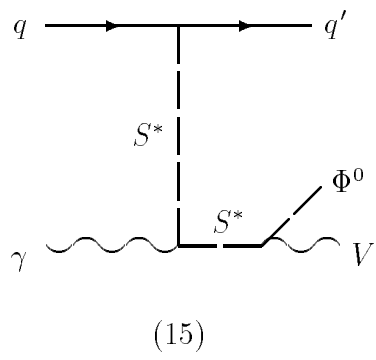
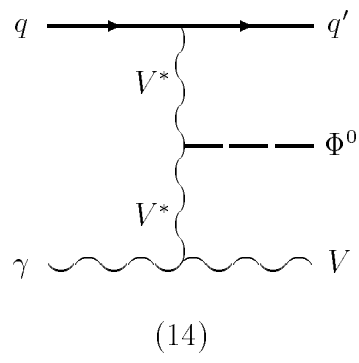
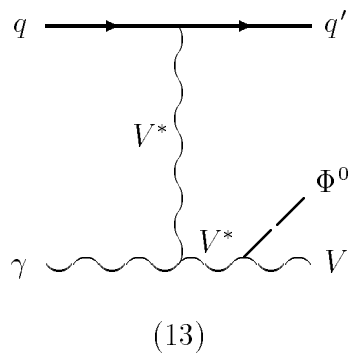
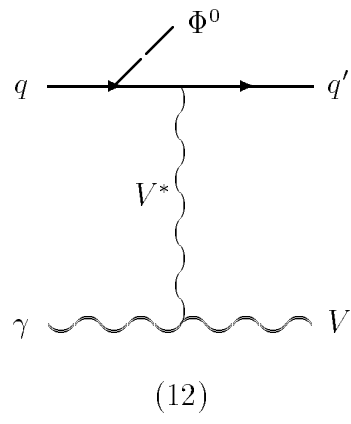
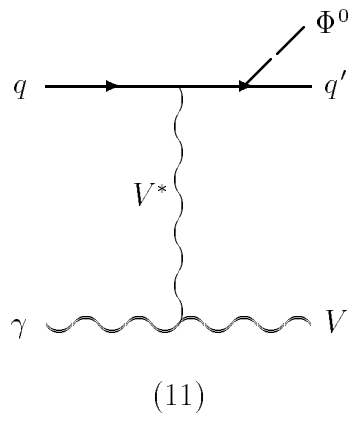
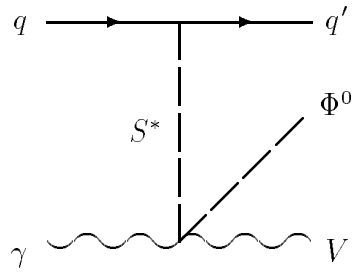


Fig.1 (Continued)



(17)

Fig.1 (Continued)

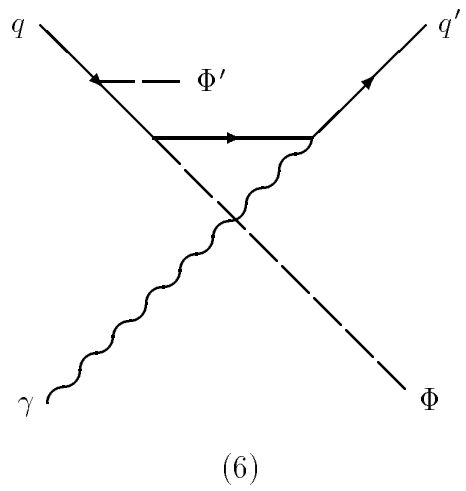
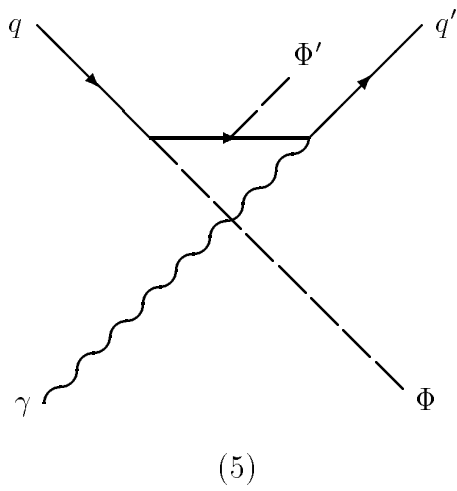
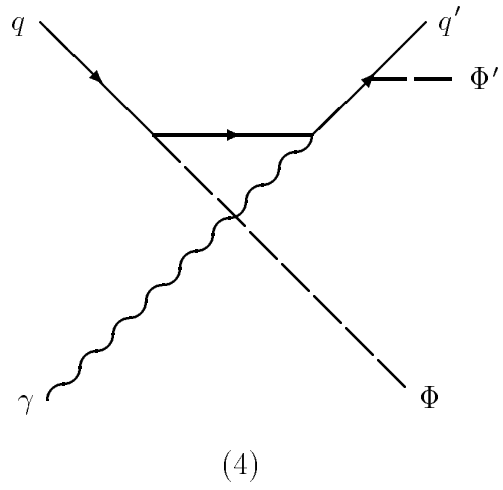
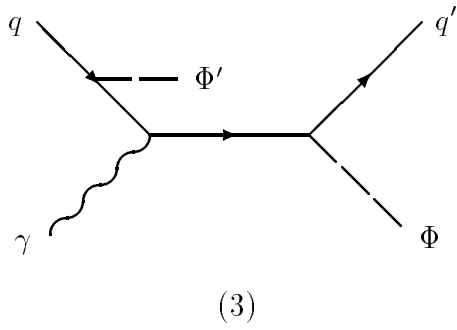
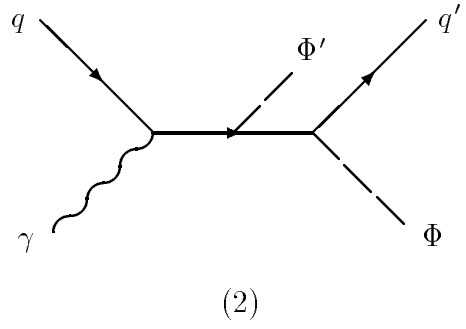
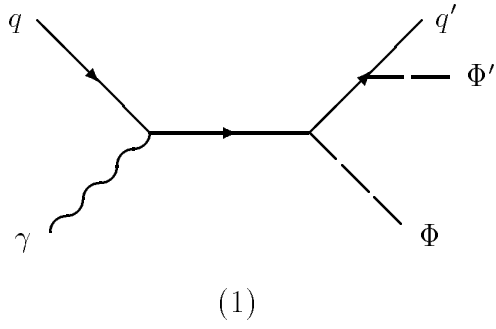
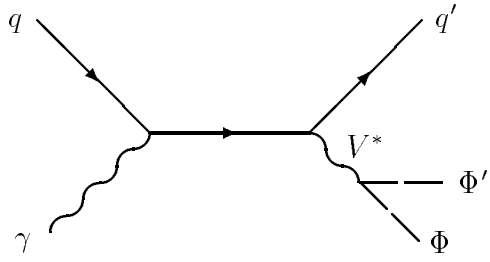
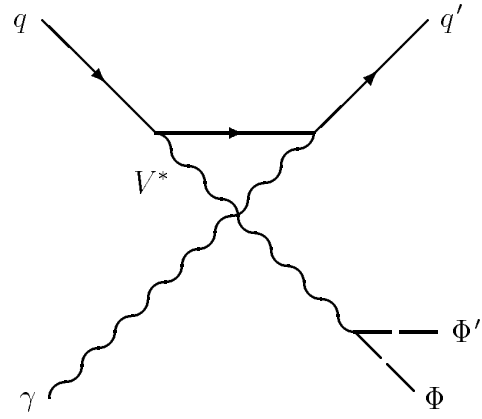


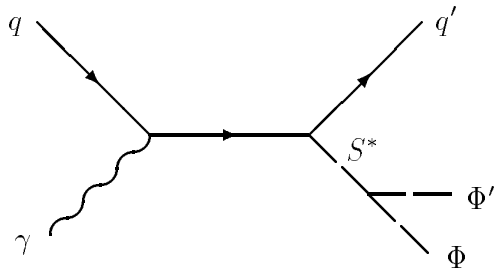
Fig.2



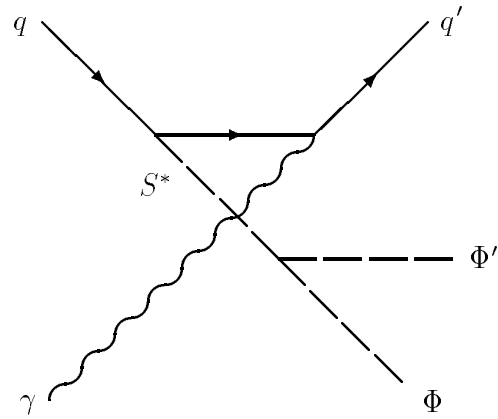
(7)



(8)

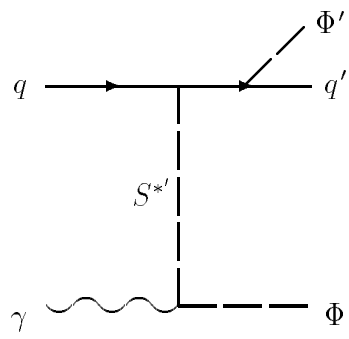


(9)

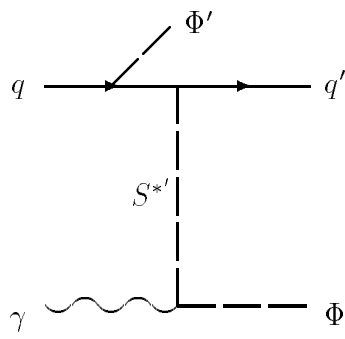


(10)

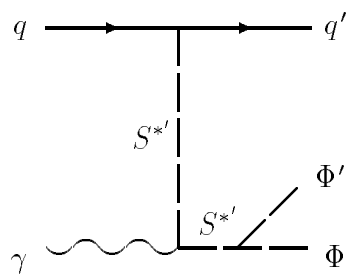
Fig.2 (Continued)



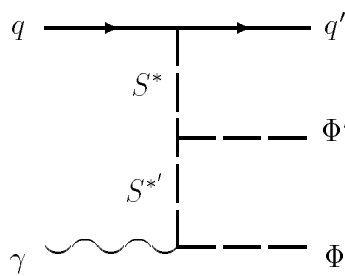
(11)



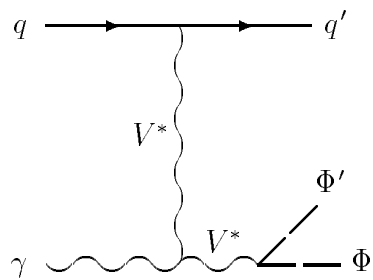
(12)



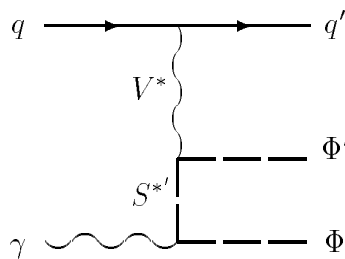
(13)



(14)

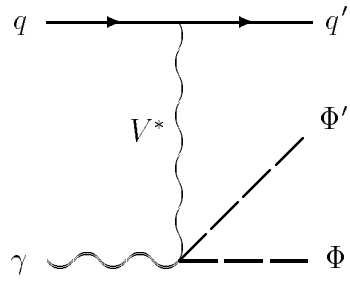


(15)



(16)

Fig.2 (Continued)



(17)

Fig.2 (Continued)

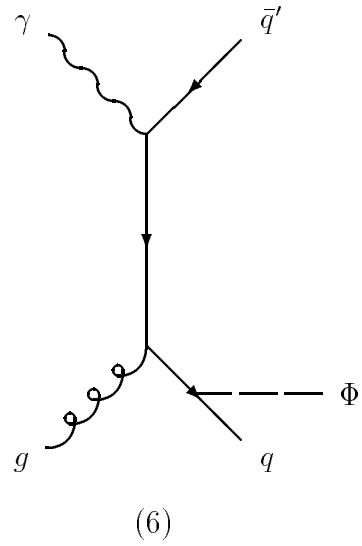
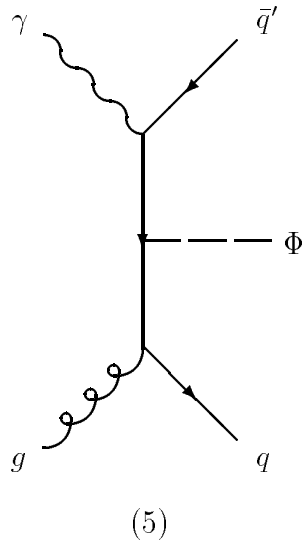
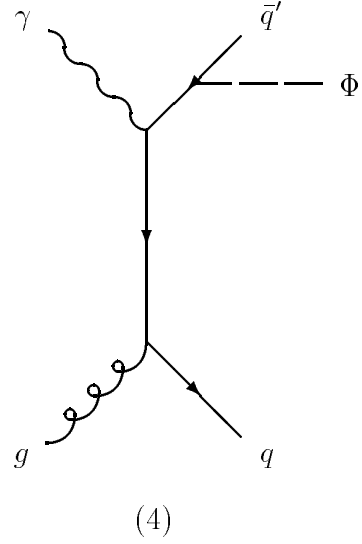
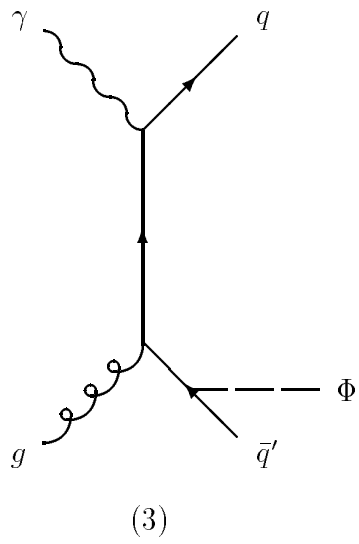
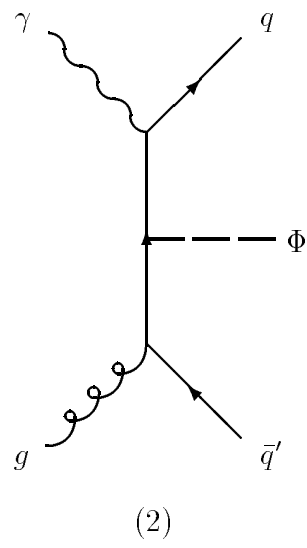
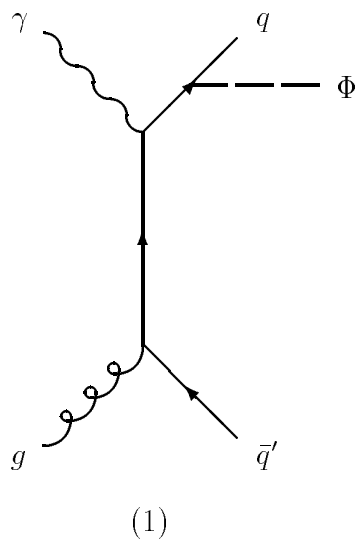
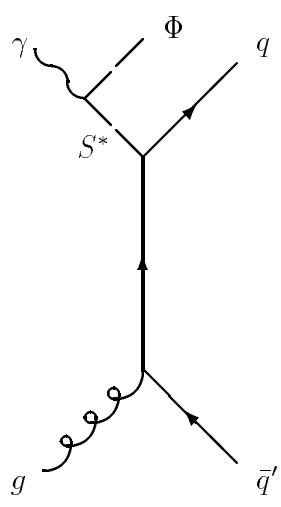
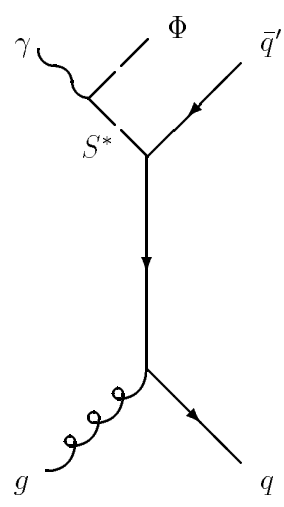


Fig.3



(7)



(8)

Fig.3 (Continued)